energies

MDPI

Review

Recent Progress on the Key Materials and Components for Proton Exchange Membrane Fuel Cells in Vehicle Applications

Cheng Wang [1,5,*], Shubo Wang [1], Linfa Peng [2], Junliang Zhang [3], Zhigang Shao [4], Jun Huang [5], Chunwen Sun [6], Minggao Ouyang [5] and Xiangming He [1,5,*]

1 Institute of Nuclear and New Energy Technology, Tsinghua University, Beijing 100084, China; wangshubo@mail.tsinghua.edu.cn
2 State Key Laboratory of Mechanical System and Vibration, Shanghai Jiao Tong University, Shanghai 200240, China; penglinfa@sjtu.edu.cn
3 School of Mechanical Engineering, Shanghai Jiao Tong University, Shanghai 200240, China; junliang.zhang@sjtu.edu.cn
4 Fuel Cell System and Engineering Laboratory, Dalian Institute of Chemical Physics, Chinese Academy of Sciences, Dalian 116023, Liaoning, China; zhgshao@dicp.ac.cn
5 State Key Laboratory of Automotive Safety and Energy, Tsinghua University, Beijing 100084, China; huangjun12@mails.tsinghua.edu.cn (J.H.); ouymg@tsinghua.edu.cn (M.O.)
6 Beijing Institute of Nanoenergy and Nanosystems, Chinese Academy of Sciences, Beijing 100083, China; sunchunwen@binn.cas.cn
* Correspondence: wangcheng@tsinghua.edu.cn (C.W.); hexm@tsinghua.edu.cn (X.H.); Tel./Fax: +86-10-6279-7595 (C.W. & X.H.)

Academic Editor: Vladimir Gurau
Received: 30 May 2016; Accepted: 11 July 2016; Published: 29 July 2016

Abstract: Fuel cells are the most clean and efficient power source for vehicles. In particular, proton exchange membrane fuel cells (PEMFCs) are the most promising candidate for automobile applications due to their rapid start-up and low-temperature operation. Through extensive global research efforts in the latest decade, the performance of PEMFCs, including energy efficiency, volumetric and mass power density, and low temperature startup ability, have achieved significant breakthroughs. In 2014, fuel cell powered vehicles were introduced into the market by several prominent vehicle companies. However, the low durability and high cost of PEMFC systems are still the main obstacles for large-scale industrialization of this technology. The key materials and components used in PEMFCs greatly affect their durability and cost. In this review, the technical progress of key materials and components for PEMFCs has been summarized and critically discussed, including topics such as the membrane, catalyst layer, gas diffusion layer, and bipolar plate. The development of high-durability processing technologies is also introduced. Finally, this review is concluded with personal perspectives on the future research directions of this area.

Keywords: hydrogen energy; fuel cell automobile; catalyst; proton exchange membrane; gas diffusion layer; bipolar plate

1. Introduction

Proton Exchange Membrane Fuel Cells (PEMFCs) are the most efficient power generation devices due to the electrochemical processes in PEMFCs are not governed by Carnot's Law, therefore, the efficiency of fuel cells is not strongly dependent on operating temperature and high efficiency can be achieved under relative low operating temperatures. PEMFCs have a wide range of applications, including electric vehicle power sources, especially their automobile application, distributed power

stations, portable power systems, etc. This review is focus on the key materials research and development progress for PEMFCs vehicle applications.

1.1. The Progress and Targets of Fuel Cell Vehicle Industrialization

Fuel cells for use in vehicles include proton exchange membrane fuel cells (PEMFCs), metal/air fuel cells, etc. PEMFCs are environmentally benign, high efficiency, and high power density electrical devices that directly convert the chemical energy of hydrogen into electricity. PEMFCs are a promising candidate for pollution-free automotive applications [1]. Through continuous global research and development (R&D) over the past decade, the important operational factors of PEMFCs, such as energy efficiency, volumetric and mass power density, and low temperature start ability, have been greatly improved. The industrialization of fuel cell vehicles is currently in progress, and some notable milestones are worth mentioning: (1) the fuel cell engine produced by Hyundai-Kia exhibited 60% energy efficiency (specific value of DC output power and Lower Heat Value (LHV) hydrogen energy) under 25% rated power [2]; (2) significantly increased PEMFC module power density was reported [3], for example, a 3.1 kW/L power density was achieved by a Japanese Toyota Sedan Vehicle fuel cell and an English Intelligent Energy EC200-192 module exhibited 5 kW/L power density; (3) 2 kW/kg specific power was achieved in Nissan using a 2011-model PEMFC module [4]; and (4) automotive fuel cells made by Toyota and Honda achieved cold starts at −37 °C and −30 °C, respectively [5]. In 2014, the Toyota MIRAI fuel cell vehicle was introduced onto the market, with a fuel cell peak power of 114 kW and a driving range of 500 km.

Although the state-of-the-art automotive fuel cell technology has achieved the abovementioned technical milestones, the durability and cost have not yet met the commercialization targets and these factors are nowadays the ultimate obstacles for widespread industrialization of fuel cell vehicles. The "Fuel Cell Technical Team Roadmap" drafted by the U.S. DRIVE Partnership in 2013 clearly described the technical and commercial targets for automotive fuel cells [6]. Figure 1 shows a diagram of the key PEMFC properties and the current status of the targets. The current system durability is generally 2500 h and system cost is 49 USD/kW (corresponding to 500,000 sets per year). It can be seen from Figure 1 that the current technology of system start from −20 °C, stack energy efficiency @ 1/4 rated power (the target is 60%), stack power density (the target is 2.5 kW/L) and specific power (the target is 2.0 kW/kg) have been already achieved the commercial targets, however it still has a long way to go to achieve the commercial targets of system durability (the target is 5000 h) and system cost (the target is 30 USD/kW), respectively [7].

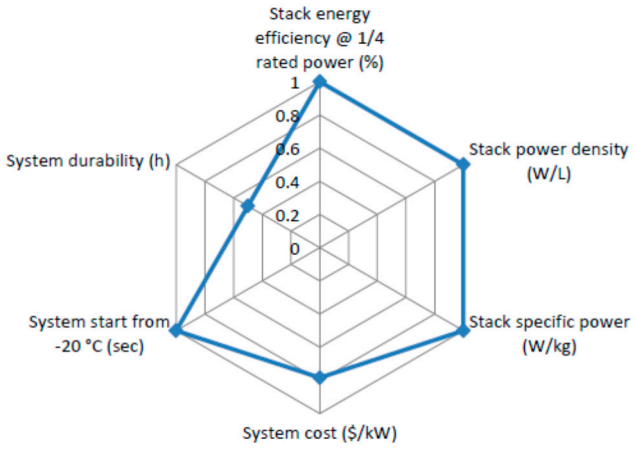

Figure 1. Diagram showing PEMFC properties and their corresponding industrialization targets. The blue line indicates the current status as a fraction of the target value.

1.2. Industrialization Targets of the Key Materials and Components for PEMFC Vehicles

R&D of novel critical materials and components has been an approach to improve the durability and cost efficiency of PEMFCs. Some key materials for PEMFC include proton exchanges membranes, catalysts, and support materials for the catalyst. The components include a proton exchange membrane (PEM), catalyst layer (CL), gas diffusion layer (GDL), and bi-polar plate (BPP). The catalyst coated membrane (CCM) comprises the membrane and catalyst layers, while the membrane electrode assembly (MEA) consists of the CCM and GDL.

The function of the PEM is proton conduction (which occurs in the presence of water), reaction gas separation, and electronic insulation. The most common membrane material used for this application is a perfluorinated acid resin. Over the past decades, the most important technological progress in the field of PEMFCs was the development of ultra-thin enhanced proton exchange membranes. The membrane thickness reduced from hundreds of microns to a dozen microns (resulting in a decrease in the electrical resistance), the membrane can be fully humidified, and the fuel cell performance was increased significantly [8]. Table 1 shows the U.S. Department of Energy (DOE) technical targets for 2020 for the key membrane properties [6]. The evaluated properties include area specific proton resistance (<20 $m\Omega \cdot cm^2$), hydrogen and oxygen crossover (<<2 mA/cm^2) and cost (<20 $USD \cdot m^{-2}$).

Table 1. U.S. Department of Energy technical targets for PEMFC membranes [6].

Characteristic	Units	Status	2020 Target
Maximum Oxygen crossover	mA/cm^2	<1	2
Maximum hydrogen crossover	mA/cm^2	<1.8	2
Area specific proton resistance (80 °C and water partial pressures from 25 to 45 KPa)	$\Omega \cdot cm^2$	0.017 (25 KPa)	
0.006 (44 KPa)	0.02		
Maximum operating temperature	°C	120	120
Minimum electrical resistance	$\Omega \cdot cm^2$	-	1000
Cost	USD/m^2	18	20
Durability	Cycles	>20,000	20,000

The catalyst layer is a porous structure consisting of the catalyst, support material, and proton conducting resin. The function of the CL is hydrogen oxidation and oxygen reduction and the thickness is typically 10–20 µm. The Pt loading in the CL is 0.3 mg/cm^2 for the anode and 0.4 mg/cm^2 for the cathode. The required Pt dosage is usually around 1 g/kW, corresponding to a total of 50 g for a car and 100 g for a bus; as Pt is an expensive part of the system, reducing the Pt dosage is a challenge [9].

Table 2 shows DOE targets for PEMFC catalyst performances [6]. The targets for Pt dosage are 0.125 mg/cm^2 and 0.125 g/kW, respectively, and the catalyst activity loss <40% under high voltage cyclic accelerated degradation testing. For the promotion of vehicle fuel cell industrialization, the development of novel catalyst and support materials, reducing the Pt dosage, and increasing the durability are important factors. For fuel cell vehicles to compete with combustion engines, the Pt dosage needs to be reduced to 6.25 g Pt for one car, 5000 h of durability needs to be achieved, and the system needs to achieve 30,000 start-stop cycles and 300,000 load cycles.

Table 2. Technical targets for electrocatalysts [6].

Characteristic	Units	Status	2020 Target
Platinum group metal (PGM) total content	g/kW rated	0.14	0.125
PGM total loading	mg/cm^2	0.15	0.125
Loss in catalytic (mass) activity (30,000 cycles at 0.6–1.0 V, 50 mV/s)	%	37	<40%
Mass activity	$A/mg_{PGM}@900mV_{IR\text{-}free}$	0.47–0.67	0.44
Non-PGM catalyst activity per volume of supported catalyst	$A/cm^3@800mV_{IR\text{-}free}$	60	300

At present, challenges related to the GDL are achieving a high efficiency of mass transfer for water and the reaction gas at high current density conditions and mass production technology for reducing the cost of GDL fabrication. According to the DOE report, the cost of Ballard's GDL production can be reduced to 4.45 USD/m^2 if the production capacity can reach 500,000 fuel cell stacks per year. Therefore, in the R & D of GDL, the development mass production technology is also a critical topic.

In the fuel cell stack, the main function of the BPP is the separation and distribution of the anode and cathode reaction gases, along with water management, heat conduction, current collection, and mechanical support. BPP materials include graphite, metals, and composites. Table 3 shows the DOE targets for metal BPP [6]. As shown in Table 3, to date, the cost and H_2 permeation have not met the targets and the others targets have been achieved better properties than the 2020 targets.

Table 3. Technical Targets for Bipolar Plates [6].

Characteristic	Units	Status	2020 Target
Cost	USD/kW	4	3
Weight	kg/kW	<0.4	0.4
H_2 permeation coefficient	Std $cm^3/(s{\cdot}cm^2{\cdot}Pa)$ @ 80 °C, 3 atm 100% RH	$<2 \times 10^6$	1.3×10^{-14}
Corrosion anode	$\mu A/cm^2$	No active peak	1 and no active peak
Corrosion cathode	$\mu A/cm^2$	<0.1	<1
Electrical Conductivity	S/cm	>100	100
Area specific Resistance	$Ohm{\cdot}cm^2$	0.006	0.01
Flexural Strength	MPa	>34 (carbon plate)	25

In this paper, we review the current state-of-the-art knowledge and technology of key materials and components for PEMFCs, including proton exchange membrane, catalyst, catalyst layer, gas diffusion layer and bipolar plates, based on the latest research articles, published progress reports and achievements, and information from relevant companies. In addition, we propose future development directions of the key material and components.

2. Proton Exchange Membranes

2.1. State-of-the-Art Proton Exchange Membranes

The perfluorosulfonic acid membrane applied in hydrogen fuel cells, which can only conduct protons in the presence of water, introduces the following limitations: firstly, the operating temperature of the hydrogen fuel cell needs to be below 100 °C. Secondly, the fuel cell stack water management is complicated. Thirdly, high purity hydrogen is needed to prevent Pt catalyst poisoning. According to

the latest literature on PEMs for hydrogen fuel cells, the studies were focused on the enhancement of proton conductivity and mechanical properties under high temperature and low humidity conditions. In particular, the proton conductivity in the anhydrous state was improved. Ultimately, all of the target membrane properties under high temperature, low humidity, and even anhydrous operating conditions have been achieved. The targets of a simplified water management module, reduced requirement for hydrogen purity, and lower overall cost of the hydrogen fuel cell were achieved through R&D of the membrane. The latest research on PEM involves high temperature membranes, including modified Nafion® and Aquivion® membranes and other novel PEM materials. These three membrane types are introduced and analyzed here.

2.1.1. High Temperature PEM

High temperature PEM are defined as those able to be operated at temperatures higher than 150 °C, while low temperature membranes can be operated only below 100 °C. Under higher temperature conditions, there is no liquid water in the inner fuel cell stack so the water management and cooling system can be simplified, the Pt loading can be reduced, and even non-Pt catalyst can be used. Furthermore, low purity hydrogen can be used (hydrogen fuel containing 3% CO can be used below 185 °C [10]) and the heat distribution can be made more uniform. At present, the phosphoric acid (PA)-doped polybenzimidazole (PBI) high temperature membrane is studied extensively. There is currently only a small amount of research into non-PBI membranes, such as polyvinylidene fluoride/polyvinylpyrrolidone (PVDF/PVP) membrane. The proton conductivity of a PBI membrane without PA doping is extremely low, only 10^{-9} mS/cm. The proton conductivity of PA doped PBI can be significantly increased and 0.1 S/cm can be attained at 150 °C. However, a proton conductivity of 0.2 S/cm for a Nafion® membrane can be attained at 94 °C [11]. Hence, the proton conductivity of PA doped PBI membranes needs to be further studied and improved. The proton conductivity can be enhanced by increasing the doping concentration of PA in the PBI membrane. However, increasing the amount of PA results in a significantly degradation in the mechanical properties of the membrane, making it difficult to be used in a hydrogen fuel cell. Therefore, a recent study focused on improving the proton conductivity and mechanical properties simultaneously, so that the PBI membrane with improved overall performance could be suitable for application in the fuel cell.

Approaches for improving the performance of PBI membranes include synthesis of the PBI composite membrane, organic-inorganic doped membrane, optimization of the molecule structure, high molecular weight membranes, and synthesis of the membrane through sol-gel methods.

Improving the PA Doping Level

The PA doping level can be increased by organic-inorganic doping and through the integrated design of the membrane and molecular structure. Hydrogen bonds can be formed between $BaZrO_3$ nanoparticles and PA [10], resulting in an increase in the PA doping level. In the $BaZrO_3$, proton transfer occurs via neighboring O ions, which leads to the proton transfer energy barrier being decreased [10] and hence an increase in proton conductivity. The maximum reported PA doping concentration level was 13 mol PA per PBI repeating unit, at 180 °C and 5% relative humidity, resulting in a proton conductivity of 125 mS/cm [10].

Silica is one of the most commonly used materials for doping. The quality of the interface between silica and the PBI polymer can be enhanced by surface modification of the silica. In Singha's study [12], the surface of silica nanoparticles were modified using a long aliphatic chain with multiple amine groups. Meanwhile, more active proton conduction sites were provided by the long chain amine modified silica (LAMS) and the proton conductivity was increased. Thereby, the LAMS modified poly (4,4′-diphenylether-5,5′-bibenzimidazole) (OPBI) exhibited enhanced mechanical properties, thermal stability, chemical stability, and proton conduction. The dynamic mechanical performance of LAMS modified OPBI was increased by 60% compared with that of the pure OPBI and the proton conductivity reached 176 mS/cm at 160 °C.

Sulfonated mesoporous organosilicate (s-MPOs) [13] has an ordered structure and many SO_3H groups are distributed on the inner porous surface. A proton conductivity of 0.21 S/cm was obtained when s-MPOs was introduced into PA doped PBI membrane, due to the excellent properties of s-MPOs. However, in this study, the conductivity was measured at 80 °C and no performance data was shown above 100 °C. The PA doped in the PBI membrane will be dissolved and removed through the liquid water below 100 °C. Therefore, the critical properties should be studied above 100 °C.

Guo et al. [14] studied non-PBI high temperature membranes. PVP contains a *N*-heterocycle as a proton accepter that can enhance the PA doping level. This group also synthesized PVDF/PVP composite membranes. The best ratio of PVDF/PVP was 20 wt % PVDF-80 wt % PVP and 93 mS/cm proton conductivity was obtained under an anhydrous environment at 200 °C.

In addition to improving the PA doping level with co-doping and forming composites, it can be improved by structural design. A fully aromatic *meta*-polybenzimidazole (mPBI) membrane synthesized by a sol-gel casting method was studied by Kelly et al. [15]. The microstructure of this membrane was modified by the sol-gel casting method compared to conventional mPBI membranes. The conventional membrane exhibited anisotropic properties due to the side-to-side stacking of the imidazole ring on the membrane surface. The sol-gel membrane exhibited isotropic properties due to the uniform ordering of the imidazole rings. Both the mechanical properties and proton conductivity of the sol-gel membrane were enhanced through this microstructural modification. The PA doping level was improved by 60% and the proton conductivity increased from 0.09 S/cm to 0.16 S/cm at 160 °C compared to the conventional membrane.

Three-dimensional (3D) porous membrane structures can be designed to improve the PA doping level; for instance, 3D polyacrylamide-graft-chitosan (PAAm-graft-chitosan) frameworks [16] and 3D frameworks of polyacrylamide-graft-starch (PAAm-g-starch) [17]. The PA can be stored in the 3D microporous structure and an extremely high PA doping level can be obtained. In PAAm-graft-chitosan 3D membranes, a 91.51 wt % PA doping level was obtained and the proton conductivity reached 0.13 S/cm at 165 °C [16].

Improving the Mechanical Properties and Durability

PTFE is a membrane substrate commonly used to enhance the mechanical properties. However, the PTFE is hydrophobic and the compatibility with other proton exchange membranes is poor. Park et al. [18] found that the compatibility between PTFE and PBI was enhanced through a pretreatment of the PTFE membrane to make it hydrophilic and a PBI/PTFE composite membrane with excellent mechanical properties and durability was obtained. The ultimate tensile strength increased from 17.54 $\pm$ 1.04 MPa to 32.65 $\pm$ 0.61 MPa. Thermal cycling stability tests showed that the open circuit voltage (OCV) degradation rate was 118% less than the pure PBI membrane. An extremely high molecular weight (from 30 to 94 kDa) PBI membrane was designed and studied by Yang et al. [19]. With increased molecular weights, the PBI membrane properties including chemical stability, swelling, mechanical strength, and proton conductivity were all improved. PBI membranes with 78 kDa molecular weights exhibited tensile strengths of 30.3 MPa at room temperature or 7.3 MPa at 130 °C and the proton conductivity reached 0.14 S/cm at 160 °C.

In summary, the modification of high temperature membranes was studied through organic-inorganic doping, developing composites, and structural design. The organic-inorganic doping method can effectively increase the PA doping level and improve the proton conductivity, where the maximum reported proton conductivity is 0.176 S/cm [12]. Composite membranes can effectively exploit the advantages of the different components and the mechanical properties, proton conductivity, and durability can be enhanced simultaneously.

2.1.2. Modification of Nafion® and Aquivion®

Nafion® membranes have a long side chain structure and are the most widely used PEMs for hydrogen fuel cells. The Aquivion® membrane has the same perfluorinated acid structure as the

Nafion® membrane, which is characterized by a short side chain structure. Comparative studies of these two commercial membranes showed that the tensile stress of Aquivion® is 15–20 MPa [20] higher than that of Nafion® at 75–140 °C and the power density of an Aquivion® MEA is on an average 100 mW/cm^2 [20] higher than that of a Nafion® MEA under 75 °C and 90 °C at 100% relative humidity (RH), at 120 °C and 40% RH, and at 140 °C and 20% RH. Furthermore, the proton transfer channel diameter of Aquivion® is small and the hydrogen permeation, which is related to the hydrogen fuel cell durability, can be reduced. Therefore, Aquivion® membranes have higher durability [21] compared to Nafion®. Thus, it is clear that the Aquivion® membrane has a potential value for fuel cell applications, especially for operation under a high temperature and low humidity environment.

In the studies undertaken between 2014 and 2015 to modify Nafion® and Aquivion®, the main modification methods included doping, developing composites, and applying pretreatments. The proton conductivity, mechanical properties and the MEA performance at high temperature and low humidity were improved, even under anhydrous conditions.

Doping

Octaphenyl polyhedral oligomeric silsesquioxane $Ph_8Si_8O_{12}$ (POSS) has the ability to retain water even at low RH levels. When POSS is functionalized with sulfonic acid groups (sPOSS), it can participate in the proton transport process. Therefore, the proton conductivity of Nafion® membrane and power density of Nafion® MEA can be increased by doping with POSS or sPOSS [22].The proton conductivity was increased from 0.14 S/cm to 0.19 S/cm at 100% RH and the power density increased from 480 mW/cm^2 to 526 mW/cm^2 at 43% RH and 80 °C [22]. Phosphotungstic acid ($H_3PW_{12}O_{40}\cdot nH_2O$ (PWA)) has a proton conductivity between 0.02 and 0.1 S/cm at 25 °C [23]; hence, the proton conductivity of the membrane can be enhanced by PWA doping. However, the PWA will gradually be dissolved out of the structure when the PWA doped membrane is applied in a hydrogen fuel cell. The PWA can be immobilized by silicon dioxide (PWA/SiO_2) and the stability of PWA/SiO_2 doped membranes can be improved [24]. The membrane proton conductivity, hydration levels, and charge transfer process in the electrode were enhanced by PWA/SiO_2 doping and the performance of the MEA was significantly improved. The peak current density of the MEA reached 710 mA/cm^2 at 0.70 V, 80 °C, and 100% RH [24].

Benzene-bridged periodic mesoporous organosilicas functionalized with sulfonic acid (S-Ph-PMO) have a nano-ordered rigid hydrophobic-hydrophilic separated structure. The proton transfer channels can be extended for several hundred nanometers with little tortuosity [25–28] and the structure can be maintained even at 500 °C [25]. Therefore, the channel structure of S-Ph-PMO doped Nafion® membranes can be maintained at low humidity conditions and the temperature stability and mechanical properties can be effectively improved. The storage modulus of a 20 wt % S-Ph-PMO composite Nafion® membrane is 2.5–15 times higher than that of pure Nafion®, while the proton conductivity is up to 1.5 orders of magnitude higher than Nafion® at 20% RH and 40 °C [11].

Composite Membranes

When investigating composite membranes for fuel cells, PVDF and PTFE are the most commonly used substrate membranes. When Nafion®/PVDF composite membranes are prepared with unmodified PVDF, the mechanical properties can be improved, however, proton conductivity did not increase [29]. The compatibility between Nafion® and PVDF can be enhanced through functionalizing PVDF with Nafion® and the overall properties of the composite membrane can be improved [30]. The interface between Nafion® and PVDF is strengthened and the proton transfer channel was formed through the inner Nafion® in the PVDF. Thereby, the proton conductivity, mechanical properties, and hydrogen fuel cell performances were improved. The Young's modulus increased from 1190 MPa to 1840 MPa, elongation at break increased from 185% to 230% and the proton conductivity increased from 42 mS/cm to 60 mS/cm at 20 °C [30].

Investigating Nafion® and Aquivion® PTFE composite membranes, it was shown that the PTFE can improve the mechanical properties, thermal stability, and reduce pinhole formation in the composite membrane [31]. Aquivion®/PTFE composite membranes exhibited a proton conductivity of 0.2 S/cm at 120 °C compared to a value of 0.094 S/cm for Nafion®211 under the same conditions [32]. In addition, a radical scavenger, such as ceria supported on sulfonated silica [33], can be doped in the composite membrane to improve the durability. Open circuit voltage (OCV) testing indicated that the durability of the composite membrane doped with a radical scavenger was seven times higher than the membrane without the radical scavenger.

The water uptake can be increased using a SiC fiber network which can be further functionalized by PA to improve the interface quality with the Aquivion® membrane [34]. Composite Aquivion® membranes were prepared with SiC web and SiC/PA. The mechanical properties, proton conductivity, and hydrogen fuel cell performance of the composite membrane and its MEA were improved. The tensile strength was increased from 13.96 MPa to 52.17 MPa, the proton conductivity improved from 0.21 S/cm to 0.24 S/cm at 90 °C and 100% RH, and the f-power density of the cell increased from 0.9 W/cm^2 to 1.2 W/cm^2 at 75 °C and 100% RH.

As Pt is a catalyst for hydrogen oxidation and CeO_2 is a radical scavenger, Nafion® can be combined with Pt/CeO_2 particles [35] or a Pt nanolayer [36] to improve the self-wetting and durability performance. In such composite membranes, the hydrogen permeating from the anode side through the Nafion® membrane can be oxidized by Pt. The hydrogen permeation can be reduced and the electrode can be humidified by the produced water; thereby the composite membrane can be operated in a low RH environment. The radicals produced during fuel cell operation can be captured by the CeO_2 and the durability of the fuel cell can be enhanced. The maximum power density of a hydrogen fuel cell using a Pt/CeO_2 doped Nafion® membrane was increased by 20 mW/cm^2 at 35% RH compared to that of pure Nafion® and the OCV test indicated that the durability can be prolonged from 80 h to 180 h [35]. In the study of Nafion® and Pt nanolayer composite membranes [36], the tensile modulus and yield strength were increased 181% and 166%, respectively, and the maximum power density increased 200% compared with the pristine Nafion®.

Other Modification Methods

The proton transfer channel in Nafion® membranes can be modified by 3,4-dimethyl-benzaldehyde (DMBA), therefore the hydrophobic-hydrophilic separated structure can be improved and the diameter of the channel can be enlarged [37]. The proton conductivity of the modified membrane shows an improvement from 22% to 34% compared with unmodified Nafion®. In addition, Napoli et al. [38] studied the performance of Nafion® membranes subjected to different pretreatments. Pretreatment using nitric and sulfuric acid resulted in proton conductivities of 0.2492 S/cm and 0.1026 S/cm, respectively. The sulfuric acid treatment gave better results than the one with nitric acid; the level of hydration of the Nafion® membrane is dependent on the type of acid and stronger hydration was obtained with nitric acid pretreatment, and hence, the proton conductivity was higher. In summary, the performance of Nafion® membranes operated under low humidity conditions was improved by doping with materials with good water uptake and catalytic properties. The PVDF and PTFE composite reinforced membranes could effectively improve the mechanical properties and durability, resulting in membranes that could be operated at high temperature and low humidity.

2.1.3. Other Membranes

Modification of Sulfonated Poly (arylene ether sulfone) (SPAES)

For the SPAES-modified membranes, the overall performances were improved through the functionalization of the main chain and side chain molecules. In the main chain modification study, the SPAES main chain was modified by fluorophenyl [39]. The dimensional stability and oxidative

durability of the modified SPAES was enhanced, the tensile strength was 47.3–64.5 MPa, the thermal stability was up to 260 °C, and the proton conductivity was 0.35 S/cm at 90 °C for 99.3% sulfonation. In the side chain modification study, Kwon et al. [40] modified the SPAES side chain with hydroxyl side groups contributing additional hydrogen bonding. Thereby, the interconnected hydrophilic clusters and the extent of hydrophobic-hydrophilic microphase separation were enhanced. However, the proton conductivity was only 0.1 S/cm at 80 °C and 100% RH, and hence the properties should be further improved through the optimization of the ratio of hydroxyl groups to other side groups.

Modification of Sulfonated Poly (ether ether ketone) (SPEEK)

The overall performance of SPEEK-modified samples was enhanced mainly by doping and blending. *n*-BuOH was introduced into the SPEEK to induce self-organization. Multiple hydrogen bonds can be formed between *n*-BuOH and SPEEK, so additional clustering of hydrophilic domains can be formed in the SPEEK microstructure and the diameter of ionic clusters increased from 1 nm to 3 nm [41]. Therefore, the proton conductivity and mechanical properties were improved; the proton conductivity increased to 0.314 S/cm at 80 °C and the tensile strength increased 35% [41]. The SPEEK was blended with fluorinated poly(arylene ether) [42] and the blended membrane exhibited enhanced thermal and chemical durability compared with pure SPEEK. However, the proton conductivity was low; only 0.1 S/cm at 80 °C and 100% RH.

Modification of Other Membranes

A grafting proton conducting membrane of poly(ethylene-alt-tetrafluoroethylene) (ETFE) and various co-monomers including styrene, methacrylonitrile (MAN), acrylonitrile (AN), methyl methacrylate (MMA), and methacrylic acid (MAA) was studied using a radiation grafting method [43]. The proton conductivity was in the range of 30–150 mS/cm at room temperature. However, better properties were not obtained using multi co-monomers and the maximum proton conductivity was achieved using a styrene co-monomer alone. An extremely high proton conductivity membrane was obtained by incorporated graphene oxide (GO) into sulfonated polyimide (SPI) where the proton conductivity was 1.2 S/cm at 80 °C and 100% RH. This can be attributed to the formation of strong hydrogen bonding interactions between the small GO and SPI, resulting in a well-defined microstructure and well-connected proton transport channels being formed [44].

Room Temperature Ionic Liquids Electrolytes

Room temperature ionic liquids (RTILs) electrolytes have attracted considerable attention in electrochemical applications [45] and can be a good candidate for high-temperature PEMFCs [46–48] application due to its more thermally stable at a wide temperature range [49,50] and non-volatile dopant than other acid doping composite membranes. Based on cationic structures, the RTILs can be classified into one of seven families [51] and it is possible to design desired physicochemical properties of RTILs by the choice of the ionic constituents. The most common cations available commercially and easier to synthesize are those based on imidazolium and ammonium [51,52]. At present, the RTILs electrolytes and their fuel cell performances need to be further improved.

In summary, the investigation of these alternate proton exchange membranes mainly focused on the modification of SPAES and SPEEK. Proton conductivities as high as 0.3 S/cm were obtained at 80 °C, superior to that of Nafion® membranes. However, the properties of hydrogen fuel cells using these membranes were not as high as the Nafion® based fuel cell. Therefore, MEA preparation technology, especially for the SPAES and SPEEK membranes, needs to be further developed and it should focus on the enhancement of durability. If this is achieved, then these membranes could be applied in hydrogen fuel cells.

2.2. Membranes for PEM Industrialization

Perfluorosulfonic membranes are the most widely used proton exchange membranes for PEMFCs. Some common commercial membranes include the Nafion® membrane produced by Du Pont (Wilmington, DE, USA), the Dow membrane produced by the Dow Chemical Company (Midland, MI, USA), the Ionomer membrane produced by 3M (Saint Paul, MN, USA), and the Aquivion® membrane produced by Solvay Solexis (Bollate, Milan, Italy). Other equivalent membranes include the Flemion® membrane produced by Asahi Glass (Tokyo, Japan), the Aciplex® membrane produced by the Asahi Chemical Corporation (Tokyo, Japan), and the Fumapem® F membrane produced by FUMA Tech (Bietigheim-Bissingen, Germany). Some perfluorosulfonic membrane product information is listed in Table 4 (as provided on the official websites of the suppliers).

Table 4. Properties of various perfluorosulfonic acid membranes.

Brand and Manufacturer	EW Value/g·mol^{-1}	Thickness/μm
Nafion® (Dupont)	1100–1200	25–250
Dow membrane (Dow Chemical)	800	125
Flemion (Asahi Glass)	1000	50–120
Aciplex (Asahi Chemical)	1000–1200	25–100
3M Ionomer (3M)	600–800	14–20
Aquivion (Solvay Solexis)	700–900	30–100
Fumapem® F (Fuma Tech)	700–1000	19–180

In Part 2.1.2, some properties of the Nafion® and Aquivion® membranes were compared. Figure 2 compares the chemical structure of these membranes showing the different side chain lengths produced by different companies. To achieve the DOE membrane targets, at present a consistent scheme proposed by these manufacturers is to prepare an enhanced composite membrane with low equivalent weight (EW) and short side chains. In order to obtain membranes with higher proton conductivities, the EW value must be reduced to 600–800. An approach to reduce EW values is to prepare multi-acid side chain proton exchange membranes, the structure of which is shown in Figure 3. However, low EW values cause membrane swelling, and the degradation of the mechanical properties, durability, and other properties. The preparation of modified membranes is an approach for obtaining low EW membranes with enhanced overall properties. The modification approaches including blending, crosslinking, and producing composites. The structures of the ionomer and nanofiber reinforced membranes, which are the focus of the development of composite modified low EW membranes by 3M are shown in Figure 3. According to the latest progress report from 3M in 2014 [53], the EW value of nanofiber reinforced multi-acid side chain membranes reached 725 and the membrane thickness was reduced to 14–20 μm. However, the membrane resistance and durability at 80 °C and 120 °C were slightly lower than the 2017 and 2020 DOE targets. The membrane impedance and hydrogen permeation performance at −20 °C and 30 °C exceeded the 2017 and 2020 DOE targets. Currently, membrane R & D in 3M is still in progress and data for complete fuel cells is not available.

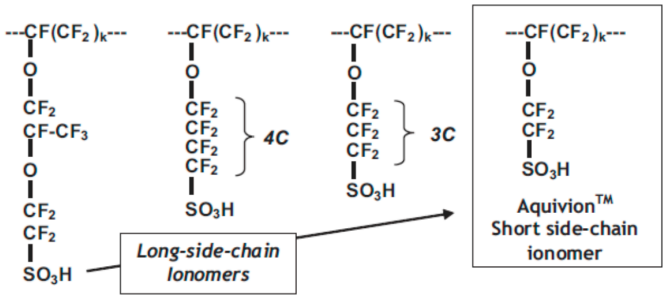

Figure 2. Chemical structure of various chain length ionomers [54].

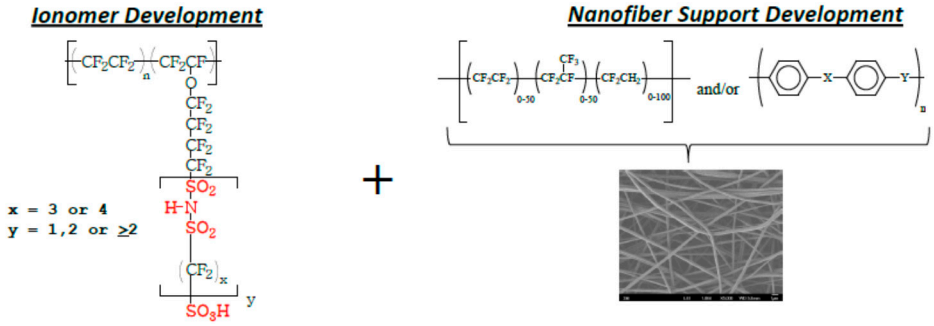

Figure 3. Structural diagrams of the nanofiber reinforced multi-acid side chain membrane from 3M [53].

2.3. Future R & D Direction of PEMs

Based on the latest membrane developments and the products on the market from various companies, the future R & D of proton exchange membranes should be focused on the preparation of composite membranes with short side chains, low EW values, enhanced mechanical properties, and increased durability. Such achievements would allow the PEMs to be operated under high temperature and low relative humidity conditions. Thus, a new generation membrane with excellent overall performance that can be applied in practical vehicles is highly anticipated.

3. Catalysts System

3.1. State-of-the-Art Catalysts and Support Materials

Currently, the leading cathode electrocatalysts are supported Pt and Pt-based catalysts. Pt alloy based catalysts, core-shell catalysts, and nanostructured thin film catalysts have been extensively studied for improving catalytic performance, including Pt utilization rates, mass and specific activity, and durability [55–57]. These Pt-based catalysts usually operate under low pH, high oxygen concentration, and high electrode potential conditions in PEMFCs. Carbon based support materials can be corroded in these environments. Consequently, Pt nanoparticles deposited onto support structures can be aggregated or dissolved from the substrate under these conditions [58,59]. Therefore, various novel catalyst support materials were studied for enhancing catalyst durability. In addition, non-Pt catalysts were also studied. Although the performance of these non-Pt catalysts was improved, they still required significant development before they are suitable for application in PEMFCs. The latest key developments on the catalysts and support materials are briefly reviewed here.

3.1.1. Catalysts

The electrocatalytic activities and stability of the Pt alloy catalysts in PEMFCs are reported to be closely related to the ability of the alloy near-surface region to retain the transition metal [60]. This might be critical to maintain the modified electronic structure of surface Pt atoms associated with the transition metal. The modified electronic structure is thought to be necessary to provide enhanced mass and specific activities relative to pure Pt nanoparticle catalysts. Furthermore, it was found that the activity of alloy catalysts could be further improved by controlling the exposed crystal facets and the composition profile of the alloy particles [55,56,61], which is promising for further reducing the Pt consumption in the fuel cells. According to a report by Chen et al., alloy catalysts based on Pt-Ni, synthesized by transforming $PtNi_3$ polyhedra in solution into Pt_3Ni nanoframes by interior erosion, achieved 36 times enhancement in mass activity and 22 times enhancement in the specific activity for the oxygen reduction reaction (ORR) during prolonged exposure to reaction conditions compared to state-of-the-art platinum-carbon catalysts. These electrochemical measurements where performed using the thin-film rotating ring-disk electrode (RRDE) method. The performance of the Pt_3Ni nanoframes is to be tested in fuel cells and is anticipated to show similar improvements as

shown by the RRDE results. Furthermore, Pt-3D-metal alloy catalysts have drawn much attention recently because of their application in automobile fuel cells. According to a recent release from Toyota, Pt-Co alloy catalysts were successfully used in the fuel cell stack of their MIRAI vehicles.

In core-shell structured catalysts, the structure of the monolayer shell showed a high utilization of Pt and therefore received much attention. According to reports by Zhang et al. [62,63], if a suitable substrate metal is selected, monolayer Pt electrocatalysts can have better electrocatalytic activity than bulk Pt. Furthermore, the activity and durability of the ORR monolayer electrocatalysts could be further enhanced by controlling the core-metal components, size, and shape [64]. The synthesized Pt monolayer catalysts on 4 nm Pd and 4.6 nm Pd_3Co cores showed mass activities of 1.0 and 1.6 $mA \cdot \mu g^{-1}_{Pt}$ at 0.9 V, and about five- and nine-fold enhancements over that of 3 nm Pt nanoparticles, respectively, tested using a rotating disk electrode (1600 rpm) in oxygen-saturated 0.1 M $HClO_4$ solutions. Kuttiyiel et al. [65] developed novel nitride-stabilized PtM core-shell catalysts (M = Fe, Co, and Ni) with low Pt content shells and inexpensive metal-nitride cores, which showed three to four times higher mass activity and three to seven times higher specific activity than a Pt/C catalyst. A schematic diagram showing the structure of this core-shell catalyst is shown in Figure 4. They further found that the N and the core-shell structure in the PtNiN nanoparticles provided an excellent stabilizing effect under highly oxidizing conditions by suppressing the dissolution of Pt during potential cycling, which showed only an 11 mV loss of the half wave potential after 35,000 cycles during rotating disk electrode tests. It has been reported that Pt monolayer catalysts, such as Pt_{ML}/Pd/NiW/GDL and Pt_{ML}/Pd/C, showed excellent durability in PEMFC tests [64], but their H_2/Air performance needs further improvement by optimizing the ionomer distribution in the catalyst layer.

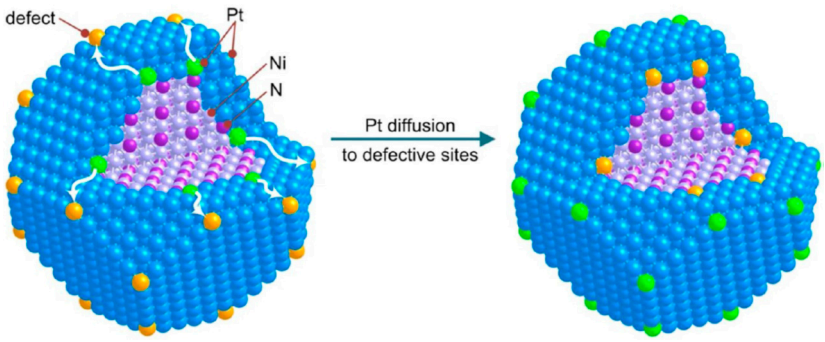

Figure 4. Structure of core-shell catalysts [66].

The 3M nanostructured thin film (NSTF) catalyst is currently the sole practical example of an extended surface area catalyst shown to effectively address several critical issues facing cathode and anode catalysts for fuel cell vehicles, including the performance, cost, and durability [67]. The NSTF $Pt_{68}Co_{29}Mn_3$ catalyst has been the workhorse cathode and anode of choice for a number of years and its CCM [68,69] generated a specific activity of 2.93 mA/cm^2_{Pt} and a mass activity of 0.18 A/mg_{Pt} at 0.9 V vs. RHE. This specific activity is around twelve times higher, and the mass activity about two times higher, than those of a TKK 47 wt % Pt/C device. However, according to the revised 2015 DOE target of 0.125 g_{Pt}/kW Pt use (down from 0.2 g_{Pt}/kW), it is likely that a new NSTF alloy material, such as a Pt_xNi_y alloy, is required. Also, the Pt_xNi_y alloys show a remarkable dependence of activity on the Ni content near composition of 70 at. % Ni. The mass activities of the NSTF Pt_3Ni_7 for ORR with standard treatment cover the range of 0.35 to 0.59 A/mg [70]. A proprietary GM additional pretreatment process can further substantially increase the mass activities over the standard treatment; 0.47 to 0.58 A/mg using the GM ORR protocol and 0.62 to 0.67 A/mg using the 3M protocol [67]. However, even though reasonable current densities are being realized at 650 mV in PEMFCs, the limiting current densities are still not optimally high. Further improvements in understanding and

controlling the dealloying and surface energy treatment processes are required in order to reach the target of 0.125 g_{Pt}/kW.

Replacing expensive Pt catalysts in PEMFC systems with non-PGM catalysts is desirable and many efforts have been made in order to reach the ultimate target for transportation applications, such as a volumetric catalyst activity $\geqslant$300 A·cm^{-3} in a MEA at 0.80 V (iR-corrected) and $\leqslant$40% performance loss at 0.80 A/cm^2 after 30,000 cycles in N_2 [71]. Although current non-PGM catalysts still have a long way to go before reaching the performance target, they are making promising progress. Serov et al. [72] recently reported a family of Fe-N-C pyrolyzed materials synthesized using a sacrificial-support method. The best of these materials showed extremely high durability in RDE tests, with more than 94% of initial activity (by $E_{1/2}$ value) after 10,000 cycles in an oxygen atmosphere and a current density of 120 mA·cm^{-2} at 0.8 V. Another breakthrough was reported by Zelenay et al. [71]. They synthesized a high-surface-area, graphene-rich polyaniline-iron-carbon catalyst through a novel three step heat treatment strategy, and achieved a current density of 0.19 A/cm^2 at 0.80 V (iR-corrected) and a volumetric current density of 84 A·cm^{-3} at 0.80 V (iR-corrected), exceeding the 2014 current density milestone (150 mA/cm^2).

3.1.2. Support Materials

The performance of a catalyst under fuel cell operating conditions is greatly dependent on the support material. The traditional carbon black support needs to be replaced or combined with other supports for PEMFC use because of its low corrosion resistance. Much effort has been devoted to developing catalyst supports, including novel nanostructured carbons, graphene, oxides, carbides, nitrides etc., and good progress has been made in recent years.

Pt-based nanoparticles supported on novel nanostructured carbon materials such as carbon nanotubes (CNTs), carbon nanofibers (CNFs), mesoporous carbon, and doped carbon, have achieved promising performance in terms of both catalytic activity and durability. They show higher catalytic performance towards ORR compared with the standard Vulcan XC-72 carbon black in many studies [73–75]. However, there are still some challenges for their widespread commercial application as PEM fuel cell electrocatalyst supports, mainly because of their higher production cost compared with carbon black.

Graphene is another promising candidate supports material for fuel cell catalysts as it exhibits high catalyst loading and good electrocatalysis and stability properties [76]. Recently, modified graphene support materials have been shown to exhibit enhanced performance. Porous graphene has been studied and the Pt catalyst with this support material exhibited 1.5 times the mass activity of non-porous graphene support materials [77]. The electrochemical activity surface area (EASA) can be increased using N-doped graphene support materials [78]. The EASA of a Pt catalyst with non-N doped graphene support material was 31.2 m^2/g and the EASA was improved to 76.9 m^2/g using N-doped graphene. Furthermore, the maximum power density can be improved using functionalized multi-walled carbon nanotubes in a graphene supported Pt catalyst [79]. The results showed that the maximum power density improved from 650 mW/cm^2 to 704 mW/cm^2. In addition, the durability can be enhanced using CeO_2 in the catalyst to quench radicals [80]. Pt/graphene and Pt/CeO_2/graphene catalysts were prepared and characterized and the results indicated that the degradation rate was 30.96 μV/cycle for the Pt/graphene catalyst and decreased to 3.61 μV/cycle for the Pt/CeO_2/graphene catalyst.

Conductive oxides, carbides, and nitrides, such as TiO_2 [47], TiC [81–83], SiC [84–86] and WC [87], have also shown promising effects on the catalytic activity and durability of PEM fuel cell catalysts. Pt supported on carbon-doped TiO_2/CNTs (Pt/C-TiO_2/CNTs) showed a better oxygen reduction activity than a commercial Pt/C catalyst. The catalyst had only <3% loss in activity after 5000 electrochemical cycles, as compared with an activity loss of about 55% for the Pt/C catalyst [57]. The activity of an Pt/ITO catalyst with an extremely high mass activity of 621 $\pm$ 31 mA/mg_{Pt} was recently reported, which is far beyond the 2015 DOE goal of 440 mA/mg_{Pt}. The stability of Pt/ITO was also very

impressive, with the EASA being unchanged and the Pt half wave potential shifting only 4 mV over 1000 potential cycles to 1.4 V vs. RHE [88]. Pt nanoparticles directly deposited onto tungsten carbide was reported by Nie et al. [89], which exhibited a much higher ORR activity than the Pt/C catalyst and a higher durability under fuel cell operation conditions. In addition, WC_x/CNTs (tungsten carbide with carbon nanotube as supports) were reported to be an efficient electrocatalyst support to reduce Pt usage, while the electrocatalytic properties of the catalyst were maintained for the ORR in direct methanol fuel cells [87]. Even though these conductive materials exhibited promising performance as supports for fuel cell catalysts, there are still some problems for practical applications related to the low surface area, low conductivity, high production cost, and instability in acidic environments. In general, these conductive materials are preferable for use as secondary supports, which work together with the primary catalyst support (usually carbon materials), to improve catalyst performance in terms of both catalytic activity and durability.

3.2. Progress of Catalyst Industrialization

Industrial mass production of catalysts has been realized by manufacturers like TKK (Tokyo, Japan), Johnson Matthey (London, UK), ETEK/BASF (Ludwigshafen, Germany), Umicore (Antwerpen, Belgium), and NEChemCat (Tokyo, Japan) and Pt/C catalysts are mainstream products. The activities of the reported commercial Pt/C catalysts, measured by thinfilm rotating disk electrode (TF-RDE) in 0.1 M $HClO_4$ and by H_2/O_2 MEA testing, where in the range of 0.11 to 0.16 A/mg_{Pt} at 0.9 V [90]. The durability of the Pt/C catalyst has also reported in the literature [91,92], showing an activity loss of about 48% after 30,000 cycles for the Pt/conventional carbon devices. Besides the Pt/C catalysts, Pt alloy catalysts, Pt-based NSTF catalysts and Pt monolayer catalysts are either commercially available or have been reported as being produced on a large-scale. The 3M Pt-based NSTF catalyst advocated by Debe [67] was reported to have a similar activity compared to Pt/C, but its performance degradation can be neglected in accelerated stress tests of PEMFCs. The activities and durability of various commercial Pt-alloy catalysts were reported by Wagner [92,93]. The average size of Pt_3Co (TEC36E52, TKK) and Pt_3Ni particles (TECNiE52, TKK) in the MEAs were estimated to be 4.9 $\pm$ 1.7 nm and 4.2 $\pm$ 1.4 nm, and their EASA values were 40 m^2/mg_{Pt} and 48 m^2/mg_{Pt}, respectively. The mass activity and specific activity of Pt_{ML}/Pd/C produced by N.E. ChemCat were reported to be 0.46 A/mg_{PGM} and 0.95 A/mg_{Pt}, respectively. Furthermore, all of these catalysts showed good electrochemical durability.

3.3. Future Direction of Catalyst Research

During the past years, the main catalyst used in automotive fuel cells has been Pt/C. In order to enhance the catalyst durability, improve the performance and reduce the cost, the Pt based alloy catalyst with core-shell or nano thin film structure and various catalyst support materials were investigated. According to a report by Toyota, because of the high activity and durability of Pt-alloy/C, it was successfully used in the fuel cell stacks of MIRAI vehicles. However, current Pt-loadings of Pt/C and Pt-alloy/C in fuel cells are still a little too high and cannot meet the cost requirement of large-scale industrialization of fuel cell vehicles. Advanced catalysts including Pt monolayer catalysts, nanometer film catalysts, controlled crystal shape catalysts, and non-PGM catalysts, are showing promising steps towards meeting the cost target. Nevertheless, their PEMFC performance and durability under vehicle operating conditions remains to be further investigated and improved.

4. Catalyst Layer

The CL is thought to be the most complex and crucial component in the PEMFC assembly for the following reasons: (1) the electrochemical reactions occur in the CL along with the transport of protons, electrons, multi-state water, and heat; (2) the complex distributions of the ionomer, carbon support, Pt particles, and pores make it extremely difficult to analyze the morphology of the CL in detail. Therefore, there has been a surge of interest and efforts in studying the connection between

microstructure, transport properties, and performance in the CL, so as to optimize its structure and decrease the Pt loading.

Initially, the membrane electrode assemblies were fabricated by hot-pressing a mixture of platinum powder and polytetrafluoroethylene (PTFE) on both sides of the proton exchange membrane. This electrode fabrication method needs a very high (and expensive) Pt loading of 4 mg/cm^2 [94]. Since then, strategies to add new components, such as a carbon support to increase the electrochemical active surface area [94] and Nafion® to furnish proton conduction [95], have been introduced and successfully decreased the Pt loading by a factor of ten, to 0.4 mg/cm^2 [96]. The second research line focuses on the development and optimization of the method for coating the catalyst layer, which is still an active research field. Pt loading and utilization in the catalyst layer can be enhanced via various coating methods, including inkjet printing [97], a combined electrospinning/electrospraying method [98], pulsed-laser-deposition [99], electrospraying of carbon-supported platinum nanowires [100], electrospraying [101], ultrasonic spraying (48 kHz [102], 120 kHz [103]), screen printing [104], and a piezo-electric printing technique [105].

Catalyst layers produced using these techniques could be called conventional CL and they have the following disadvantages: (1) Inefficient Pt utilization [106] since the Pt catalyst particles inside the agglomerate are barely accessible to the Nafion® and oxygen, leading to the absence of the three-phase boundaries needed to use the catalyst; (2) High reactant diffusion resistance due to the traditional CL being highly tortuous and significant voltage losses occurring during the transport of the reactant gas and protons to the active sites located deep inside the agglomerates, especially at high current densities. Consequently, Pt particles agglomerate, resulting in the loss of active surface area.

To overcome the above problems, new generation electrodes, namely ordered CLs have been proposed [107], developed, widely studied in the laboratory [108–123], and even commercialized [124,125]. In this section, the recent progress in the fabrication of CLs, the efforts to resolve and optimize the microstructure, and new trends in CL designs are reviewed.

4.1. State-of-the-Art Catalyst Layers

4.1.1. Gradient Design of Catalyst Layer

Various CL gradient designs have been studied and discussed here with respect to the research type (numerical, experimental, or both), gradient (Nafion® content, Pt loading, or both), and direction of the gradient design (in-plane, cross-plane, or both). From all these numerical and experimental studies, the well-acknowledged beneficial gradient distributions are: (1) an increase of the Pt loading and Nafion® content from the GDL side to the PEM side [126–131]; (2) a decrease of Pt loading from the cathode inlet to outlet [132,133]; and (3) more Pt loading under the channel than the rib [129,134].

However, it is worth noting that the effect of gradient design depends on the operating conditions. Lee et al. [135] found that under fully humidified conditions, the PEMFC with a gradient CL in which the catalyst concentration decreased from the air inlet to the outlet had a worse performance compared to a uniform sample. However, under non-humidified conditions, this gradient catalyst coating method increased cell performance by 17% at 0.8 A/cm^2. To understand these above results, one needs to take into account water management. For example, under fully humidified conditions, more Pt near the air inlet produces more liquid water and may cause flooding that reduces the performance.

Although numerous efforts have been taken to optimize the cell performance using gradient designs since 2000, it is certain that further explorations are needed, especially regarding the following aspects: (1) Simultaneous optimization of the Nafion® content and Pt loading. The strong interactions of the Nafion® and Pt catalyst distribution have been elucidated numerically by Song et al. [126], indicating that the Nafion® content and Pt loading should be optimized simultaneously. Recently, Cetinbas et al. numerically demonstrated a two-variable optimization in terms of Nafion® content and Pt loading, resulting in better performance than the single-variable optimization [136]; (2) Multiple-dimensional optimization. Most of the existing studies focused

exclusively on in-plane or cross-plane designs, and a comprehensive consideration of the in-plane distribution and the cross-plane distribution is rare [134,136]; (3) Gradient design for ordered CLs. Ordered CLs have been shown to reduce Pt loading. Since ordered CLs have a different structure from conventional CLs, the gradient design of the ordered CL maybe a future research direction. To the best of our knowledge, no such example has been published yet.

4.1.2. Ordered Design of Catalyst Layer

Ordered CLs can be broadly divided into three types: (1) ordered carbon phase, such as ordered carbon nanotubes [109,113,120,121], ordered carbon nanofibers [117,137], and ordered mesoporous carbon [112,116,119,122,123]; (2) ordered Nafion® nanofibers [115,118]; (3) ordered Pt thin film [124,125] or network [110].

Middelman [107] was one of the first to propose the idea of an ordered electrode. In this ideal electrode, the electron transport path is oriented perpendicular to the membrane. Pt catalyst particles with a particle size of approximately 2 nm were finely dispersed on the surface of the electron conductor. Then, the catalyst-coated, oriented electron conductor is coated with the ionomer for proton conduction. In this regard, all the three-phase transport paths are ordered and perpendicular to the membrane.

Out of all the ordered CLs, one outstanding type is 3M's NSTF catalyst [124,125]. In the NSTF, the catalyst support consists of highly-oriented crystalline organic whiskers, onto which the Pt or Pt-alloy catalyst is sputter-coated as a polycrystalline thin film [124,138]. Figure 5 shows cross-sectional SEM images of an NSTF electrode. One can notice that the thickness of the CL is smaller than 1 µm. It has been demonstrated that the NSTF electrode has superior Pt utilization and durability than standard electrodes [124,125].

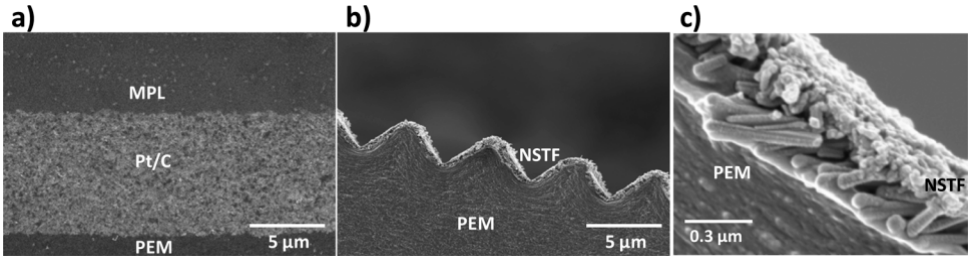

Figure 5. Cross-sectional SEM images of (**a**) conventional Pt/C electrode and (**b**) NSTF electrode; (**c**) Detailed structure of the NSTF electrode at higher magnification [138].

One major challenge in understanding the principle of the NSTF electrode is the proton conductivity mechanism. The NSFT whiskers are coated with a Pt film, and there is no ionomer in the NSTF electrode, which is analogous to Pt black electrodes. Figure 6 shows the proton conductivity of the Pt whisker, which was estimated by fitting the experimental data with a numerical model [138] as a function of the relative humidity. One can see an enhancement in the proton conductivity in the NSTF electrode compared with pure water and a significant effect of the relative humidity on the proton conductivity. To explain this ionomer-free proton conductivity phenomenon in the NSTF electrode, two possible mechanisms have been proposed in the literature: (1) diffusion of absorbed protons [139,140] and (2) electrostatic interaction between Pt and protons [141–143].

McBreen [140] reported for the first time that platinum surfaces without direct contact to the solid polymer electrolyte could take part in the electro-catalytic H-adsorption/desorption reaction under certain conditions. This phenomenon was later explained by Paulus et al. [139] in 2003. That is, the diffusion of adsorbed hydrogen along the pore/channel walls can contribute to the proton transport, which is also a plausible mechanism in the NSTF electrode.

Another possible mechanism was proposed by Chan and Eikerling [141–143], who contended that under capillary equilibrium conditions, the nanoscale, hydrophilic pores in an NSTF electrode should

be fully flooded with water. Therefore, protons would undergo bulk-like transport via the connected water film by structural diffusion. In addition, it is further postulated that the proton concentration distribution within the water-flooded pores is determined by the electrostatic interactions between the protons and the surface charge of the pore walls [141–143]. However, Sinha et al. [138] pointed out that, in their study, the NSTF electrode was found to be free of bulk liquid water. They also argued that previous studies using other surfaces such as gold or carbon in liquid water did not show similar proton conduction. To date, the mechanism of this type of proton transport remains an open question.

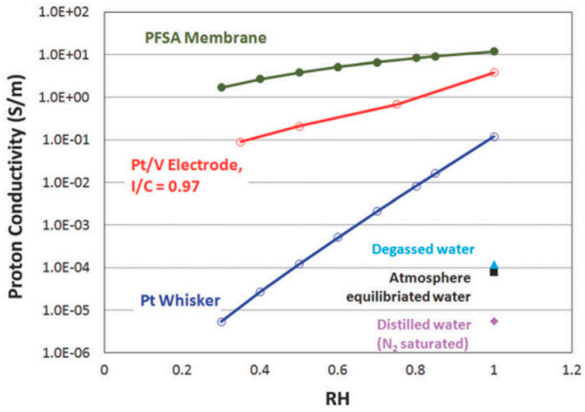

Figure 6. Estimated proton conductivity of Pt whiskers at 80 °C as a function of relative humidity, compared with the proton conductivities of a bulk membrane and that of conventional electrode with I/C of 0.97 at 80 °C and that of distilled water at 25 °C [138].

Due to the extremely thin films, much more water is generated per volume for the NSTF electrode. As a result, water management becomes a key issue, especially at low temperatures. For conventional electrodes, the water is removed through the cathode. However, for the NSTF, an 'out the anode' water removal method is proposed as a better water management strategy. To facilitate this, a thinner membrane, improved anode GDL, and differential pressures have been used [144].

5. Gas Diffusion Layer (GDL)

5.1. State-of-the-Art GDL

One of the influencing factors on the performance of hydrogen fuel cell is the water-thermal management, which is closely related to the performance of the GDL. The GDL plays an important role in the transfer process of the reactant, product and electron. Through the GDL, the hydrogen and oxygen (or air) are transferred from the bipolar plate (BP) to the catalyst layer (CL). The product water is transferred from the CL to the flow field of the BP and excreted from the fuel cell. Simultaneously the proton exchange membrane is maintained at a certain relative humidity (RH) and conducts the electrons generated by the chemical reaction in the CL. To exclude excess water and maintain the required RH condition is very important. Excessive water will occupy the pore structure of the GDL and the active sites of the CL. The reaction gas transfer process can be restrained in the GDL and the contact between the reactant gas and the CL can be also impeded and the electrochemical reaction will not be efficient. On the other hand, the proton conduction mechanism in the Nafion® membrane depends on the presence of water; if the RH is reduced or the membrane is dehydrated, the proton conductivity of the membrane will decrease and the impedance will increase. Irreversible degradation of the Nafion® membrane will result and the fuel cell durability will be decreased. Consequently, the overall performance of hydrogen fuel cells is closely related to the performance of the GDL. The GDL has a small impact on the Ohmic polarization and a critical influence on the mass transfer polarization [145]. When the fuel cell is operated at high current density, a large amount of water will be generated, the GDL porous structure will be filled with water and the reactant gas and product water

cannot be effectively transported. In this situation, the GDL drainage is critical to the performance of the hydrogen fuel cell; improving the drainage properties can increase the maximum current and power density of the fuel cell.

Based on these requirements, a GDL typically consists of a porous substrate material (such as carbon paper or carbon fiber cloth) and a single- or multi-layer microporous layer (MPL) prepared on the surface of the substrate material. The hydrophobicity of the substrate materials can be enhanced by the MPL and the drainage performance of the GDL can be improved. The substrate is the support material for the MPL and is pretreated to be hydrophobic. The MPL is comprised of a carbon powder and hydrophobic agent (such as PTFE).

However, in the practical application of GDLs in the assembled fuel cells, the porosity of the GDL at the under-rib site is reduced [146] by the assembly pressure. Thereby, the mass transfer property [147] and water distribution [148] properties are reduced. The GDL water distribution at both the under-rib and under-channel region were studied by Lee [148]. The water at the under-rib region cannot be efficiently discharged and the water is removed through the under-channel region (which dominates the mass transfer properties). In a numerical investigation, the porosity was enhanced by Cheema et al. [147] and the performance of the fuel cell was improved. Therefore, in addition to the GDL materials, studying the GDL structure is critical to enhancing the fuel cell performance.

According to the latest studies on GDLs for hydrogen fuel cell application, retrieved from the Web of Science between 2014 and 2015, the studies were mainly focused on the pretreatment technology for substrate materials, the preparation of MPLs, and the structural designs of GDL.

5.1.1. Pretreatment of GDL Substrates and Preparation of Hydrophobic MPL

Typically, the substrate materials, such as carbon paper, are immersed into a PTFE emulsion for pretreatment. The PTFE loading are unevenly distributed in the pores or on the surface of carbon paper [149] due to the residual air in the pores. In order to improve the uniformity of the PTFE distribution and the hydrophobicity of the substrate material, the pretreatments were carried out under vacuum by Song et al. [150] to remove the residual air in the pores so that the PTFE can be evenly distributed in the pores (resulting in improved hydrophobicity of the GDL). These results showed that the water contact angle decreased with the vacuum pretreated carbon paper as more PTFE was immersed in the micropores of the paper.

In addition to the effect of the uniformity of PTFE distribution on the performance of GDL, the content of PTFE in the substrate and the MPL is also critical to the performance of the GDL. The concentration of PTFE affects the GDL drainage properties [151], binding energy between the MPL and substrate [152], oxygen transfer process [153], water distribution [153], porous structure, and contact angle [149]. The contact angle was significantly increased by the PTFE pretreatment; however, further increases in the PTFE content had little impact on the contact angle [151]. Although the contact angle cannot be improved by large increases in the PTFE content, the drainage property of GDL can be enhanced and the less diameter droplet can be drained [151]. Increasing the content of PTFE in the MPL can increase the interfacial fracture energy between the MPL and the substrate material [152], as the interaction between substrate and MPL can be strengthened by the higher PTFE content in substrate. Therefore, the MPL is difficult to separate from the substrate and the GDL durability can be increased. Hydrophobic transfer channels are formed through the PTFE through which the reactant oxygen is transported. However, gas transfer channels can be occupied by excessive PTFE and the transport process can be degraded. Hence, the oxygen transfer process can be enhanced by optimization the PTFE content [153].

In addition to studying the PTFE hydrophobic agent, novel GDL hydrophobic additives were also investigated in detail. Polydimethylsiloxane (PDMS), used as a superhydrophobic layer, was deposited on carbon paper (SGL 10BC GDL) by chemical vaporous deposition (CVD) [154] and a GDL with a superhydrophobic surface was obtained. The contact angle of substrate was 134.7° which increased

to 150.9° after depositing the superhydrophobic layer. The fuel cell test showed that the maximum power density and current density were increased to 100 mW/cm^2 and 200 mA/cm^2, respectively.

Latorrata et al. [155] prepared a MPL with fluorinated ethylene propylene (FEP), carbon nano-tubes (CNTs) and carbon powder. The heat treatment temperature was reduced from 350 °C to 260 °C using FEP and the Ohmic resistance was reduced using highly conductive CNTs. In Gola's study [156], carbon cloth was used as a substrate and linear perfluoropolyether (PFPE) peroxide was used as a hydrophobic material. The PFPE content was only 0.24–1.03 wt % and hydrophobicity was observed up to a PTFE content as high as 10%. This can be attributed to the PFPE chains being linked on the surface and the carbon fiber being wrapped almost completely by PFPE.

5.1.2. GDL Structure Optimization and Novel GDLs

The fuel cell performances were enhanced through the optimization of the GDL structure, GDL substrate, and MPLs. A novel GDL with triple MPLs was studied by Kitahara et al. [157]. The three MPLs include two hydrophobic layers and one hydrophilic layer, and the hydrophilic layer was coated on the double hydrophobic MPLs. The humidity of the MEA can be conserved at low humidity conditions by the hydrophilic layer and it can prevent membrane dehydration. Any excessive water can be removed at high humidity conditions by the two hydrophobic layers. Therefore, the MEA with the triple MPLs can be operated under both high and low humidity conditions.

A novel GDL with double side MPLs was studied by Huang and Chang [158]. The performance of this GDL was optimized through the MPL and PTFE content on both GDL sides. The results showed that the fuel cell performance was enhanced under low humidity conditions and the maximum power density exhibited an 85% increase compared with the conventional GDL with a single-sided MPL. However, the contact of the MPL to the bipolar plate was prone to delamination, so the interface on this side needs to be further strengthened in order to enhance the durability.

In order to improve the drainage properties of hydrogen fuel cells at high current density, a novel structured fuel cell was designed by Tanaka et al. [159]. In this novel structure, the flow field was prepared by corrugated mesh and the MPL was prepared directly on the catalyst layer, the corrugated mesh contact to MPL directly and the traditional GDL was omitted. The results showed that the water flooding at high current density was obviously decreased and exhibited 1.35 W/cm^2 peak power density. However, the high frequency resistance of 100 mΩ·cm^2 was higher than that of the traditional structured fuel cell, because the contact area between the corrugated mesh and MPL was smaller and the Ohmic resistance increased. Therefore, further studies to decrease the resistance are required.

Under practical fuel cell operating conditions, typical carbon material based GDLs can be corroded since the operation time is prolonged. In order to improve the inherent durability of GDLs, a titanium foam GDL was studied by Choi et al. [160]. These results indicated that the Ti foam with a 3D structure is superior for the catalytic reaction and it exhibited stronger corrosion resistance compared with carbon based GDLs. Also, its thickness and weight showed almost no changes during accelerated corrosion tests. Therefore, the fuel cell durability can be prolonged by applying the titanium foam GDL.

A novel TiVCr hydrogen storage alloy-coated GDL was studied by Fang et al. [161]. The fuel cell applying this GDL can be continuously operated for around 10 min at 0.6 V, in the situation close to the hydrogen fuel supply, because a certain amount of hydrogen can be stored in the TiVCr hydrogen storage alloy. The polarization curve can also be enhanced using this GDL and its power density exhibited a value 43.67% higher than the fuel cell at 65 °C without the this new GDL. However, a contact angle test indicated that the GDL surface become hydrophilic because it was functionalized with this TiVCr hydrogen storage alloy and was prone to water flooding with prolonged operation times.

5.2. The Industrialization Progress of GDLs

The GDL is generally composed of substrate materials (carbon or carbon fiber cloth) and a microporous layer (MPL) on the surface of substrate materials. Some representative GDL products and their manufactures include Sigracet GDL produced by Sigracet (Wiesbaden, Germany), a GDL

produced by Freudenberg (Weinheim, Germany), Spectracarb GDL produced by Engineered Fibers Technology (Shelton, CT, USA), a AvCarb GDL from Ballard Material Products Inc. (Lowell, MA, USA), and ELAT® produced by FuelCellsEtc (College Station, TX, USA). In addition, Toray carbon paper substrate material without MPL is produced in Japan by Toray (Ishikawa-ken, Japan). Some specifications of GDL products and manufactures are listed in Table 5 (sourced from the companies' official websites).

Table 5. Properties of various gas diffusion layers.

Brand and Manufacturer	Total Thickness/μm	Resistance/mΩ·cm^2	Areal Density/g·m^{-2}
SGL Group (Sigracet® GDL)	105–325	4–12	40–125
Freudenberg (H series GDL)	150–290	4–10	65–150
Engineered Fibers Technology (Spectracarb™ GDL)	127–381	-	-
AvCarb (AvCarb GDL)	184–330	14–17	60–185
FuelCellsEtc (ELAT®GDL)	406–490	0.1–0.17	130–250
Toray Company (Toray Carbon Paper)	110–370	4–80	-

5.3. Future R & D Directions of Gas Diffusion Layers

Based on the latest GDL studies and product information from the above manufactures, the future GDL R&D can be summarized as follows. In the field of traditional carbon based GDLs, the R&D mainly focuses on novel hydrophobic MPLs with new high-performance non-PTFE hydrophobic ingredients having uniform distributions. This is achieved through the design of novel structured GDLs and optimizing the GDLs to maintain high efficiency mass transportation characteristics even when the GDL under-rib section is deformed by the flow field. In order to further improve the GDL mechanical and durability properties, R&D of novel non-carbon based GDLs, such as foam metal GDL, is being undertaken. Thus, the peak current density and durability of fuel cells operated under high humidity and low humidity conditions can be enhanced.

6. Bipolar Plates

Bipolar plates are one of the most important components of PEMFCs, since they determine the flow field for the gases, separate the cathode and anode gases, and conduct electrons. Traditionally, the most commonly used material for BPPs has been graphite, because it has excellent corrosion resistance, low bulk density, and high electrical conductivity. Due to the different bonding characteristics of the basal plane and the layers, graphite exhibits structural anisotropy and possesses highly directional properties, e.g., thermal, mechanical and electrical conductivity [162]. Depending on the raw material used and the heat treatment process, the characteristics of synthetic graphite usually differs from each other [163]. Problems with such graphite BPPs include brittleness and a porous structure, along with the extra cost associated with machining the gas flow channels into the plates [164]. Due to the porous nature of graphite, post-processing (such as resin impregnation) is usually required to render the plate impermeable to fuel and gases [165]. In addition, graphite lacks mechanical strength and has poor ductility, which limits the minimum plate thickness to about 5–6 mm. Machining is usually employed to fabricate the flow channels in the BPPs. Machining graphite into complex designs is highly expensive and time-consuming, and therefore makes it unpractical for the full scale commercialization of fuel cells [166,167].

Therefore, composite BPPs and metallic BPPs have been designed to replace graphite plates due to their excellent mechanical properties with low manufacturing costs. These two kinds of BPPs will be systematically discussed and summarized in this section.

6.1. State-of-the-Art Progress on Bipolar Plates

6.1.1. Composite BPPs

An alternative to graphite plates is composite BPPs consisting of graphite fillers and polymer resin, which are fabricated via conventional polymer processing methods. Composite BPPs have been the subject of intense study with the focus on their electrical conductivity and mechanical properties to meet the US DOE target [168,169].

There are two types of polymer that can be used in composite BPPs, thermoplastics and thermosets. Thermoplastics include polypropylene (PP), polyethylene terephthalate (PET), and polyvinylidene fluoride (PVDF). These generally have lower glass transition temperatures (T_g) which restricts their use in high temperature fuel cells. The thermoset plastics include vinyl esters, epoxy, and phenolic resins (resole and novolac types). They are irreversibly cured using heat or via chemical reactions, so they are more suitable for high temperature composite BPPs. In addition, intrinsically conducting polymers (ICPs) such as polyanilines (PANI), polypyrroles, and polyphenylenes have been used for conductive composites due to their much higher conductivity than other polymers.

Researchers at Oak Ridge National Laboratory developed carbon/carbon composite BPPs with in-plane electrical conductivity of 200–300 S/cm and excellent mechanical properties, although the process was found to be somewhat complicated and costly for certain applications such as automotive [170]. Baird and coworkers [164,171] developed graphite-based wet-lay composite BPPs of polyphenylenesulphide (PPS). The in-plane conductivity was higher than 200 S/cm and the through-plane conductivity was 19 S/cm. A novel woven nanocomposite for BPPs was proposed by Taherian and Nasr [172]. Kim et al. [173] proposed new BPPs made of plain weave carbon fiber epoxy composite, which were developed to increase the manufacturing productivity of fuel cells and to decrease the bulk electric resistance. The prepreg surfaces were coated with graphite foils (BD-100, Samsung CNG, Cheonan, Korea) as shown in Figure 7. Two 150 mm layers of expanded graphite were placed on both surfaces of the prepreg. This process was repeated and the thickness of the graphite coating layer was controlled to 2–100 mm.

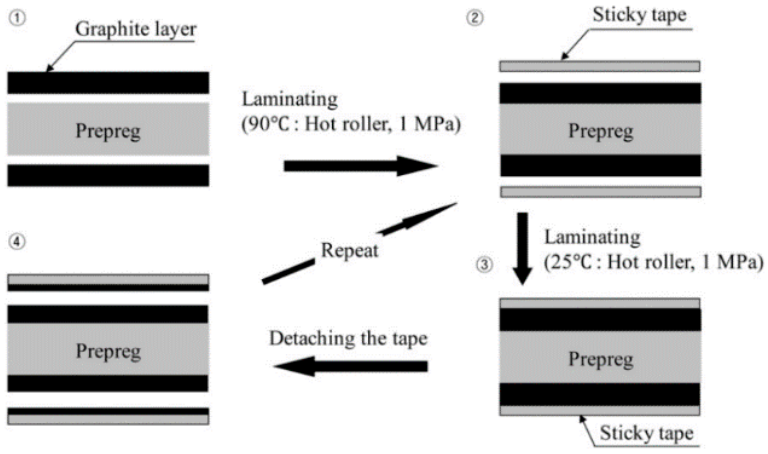

Figure 7. Schematic drawing of graphite coating method [173].

Metal-based polymer composites are a small group of composite materials that have been investigated for BPP applications. The Los Alamos National Laboratory has developed metal based composite BPPs based on porous graphite, polycarbonate plastic and stainless steel (SS) [174]. Since producing porous graphite plates is not as time consuming or expensive as producing non-porous graphite plates, the former can be used while the impermeability was provided by the SS and polycarbonate parts. SS also provided rigidity to the structure while the graphite resists corrosion. Kuo et al. [175] studied new BPPs using a composite material comprising Nylon-6 and SS316L alloy

fibers. The PEMFC plates were fabricated via an injection molding process, which yielded better production rates than coating or treating metal plates with a suitable surface material. In addition, NedStack [176] developed a two-component molding process especially for fuel cell plates. A highly conductive compound was used for the active area, while for the broader area a non-conductive injection molding grade polymer was used.

6.1.2. Thin Metallic BPPs

In recent years, thin metallic BPPs have been attracting widespread attention in the research community because of their excellent characteristics, such as high electrical conductivity, gas impermeability, high mechanical strength, and high durability to shock and vibration. Moreover, their excellent mechanical properties allow for fabrication of thinner plates. However, the metals are more susceptible to corrosion, which can adversely affect their performance and durability, thus surface pretreatment is needed to improve the anticorrosion performance.

Base Material

So far, metals such as SSs, aluminum alloys, titanium alloys, nickel alloys, copper alloys, and metal-based composites have been used in the fabrication of BPPs. Different substrates and coatings will be discussed below.

Stainless steels have attracted considerable attention due to their relatively low cost, high strength, and suitability for mass production. SSs devices can be fabricated as thin as 0.1–1 mm, which offers tremendous improvement in the power to volume and power to weight ratios. Using SS BPPs, cost estimates published in a Fuel Cells for Transportation Report 1998, showed that a typical 70 kW PEMFC stack with a cost less than USD20 kW^{-1} could be achieved [177], below the DOE target for a fuel cell set at USD30 kW^{-1}. Typically, SS consists of austenite SSs and ferrite SSs. The elements in SSs such as Cr, Ni, and Mo can create the passivation layer on the substrate surface in the acidic PEMFCs environment [178]. The criterion to select SSs for BPPs applications sharply depends on the chemical composition of material as the nature and content of the alloying elements strongly influencing the composition of the passive film formed on the metal surface, which in turn affects its overall corrosion resistance [179]. Hornung and Kappelt [180] ranked different iron-based materials in accordance with the pitting resistance equivalent $PRE = \%Cr + 3.3 \times \%Mo + 30 \times \%N$.

Aluminum may be considered for BPPs applications in PEMFC on account of the low manufacturing cost. It is reported that aluminum and its alloys do corrode in the fuel cell environment which results in the decrease of cell output performance [181]. Joseph et al. [182] deposited PANI on 6061 Al alloy to prepare BPPs and the results showed that the corrosion resistance was greatly increased compared to that of an uncoated substrate.

Ti is a lightweight metal with a density of 4.51 g/cm^3. A non-conductive oxide layer is easily formed on the Ti substrate. The non-conductive oxide layer remarkably increases the ICR. Davies et al. [183] studied the increase in the surface resistivity from an insulating oxide film on titanium plates in a single cell. Zhang [184] prepared Ti-Ag film on TA1 titanium for BPPs by arc ion plating.

Nickel is a widely available material, which exhibits excellent ductility and manufacturability. However, few investigations were found on nickel BPPs due to the relatively high cost. Wei et al. [185] performed contact resistance and corrosion resistance measurements on nickel and commercial nickel-clad BPPs. Paulauskas et al. [186] investigated the corrosion behavior of nitrided Ni-50Cr BPPs and found that the corrosion current densities were inferior to the DOE target for specimens nitrided at 1100 °C for 2 h under pure N_2.

Copper alloys are not appropriate for BPP materials for PEMFCs due to their high density. However, merits such as high electrical conductivity, chemical stability, and easy manufacturing can make copper alloys attractive for BPPs. Nikam et al. [187,188] have investigated the corrosion resistance of C-17200, a copper-beryllium alloy, in a simulated PEMFC environment.

Surface Treatments and Coating

Chrome enrichment is a widely used method to improve the corrosion resistance and current conductivity of SS BPPs using various techniques. Lee et al. [189,190] proposed an electrochemical surface treatment of SS BPPs to improve their corrosion resistance and minimize the formation of a thick oxide layer that increases the ICR during operation. Cho et al. [191] chromized SS316L by a pack cementation technique and examined the potentiodynamic and potentiostatic performance of Cr-rich layers in the pack cemented SS. The chromized SS, with 2.5 h cementation, exhibited low current density and stable polarization behavior. Later, the same authors [192] used another pack cementation process to produce corrosion resistant chromized SS316L BPPs. Feng et al. [193,194] tried to improve the performance of 316L SS BPPs using ion implantation to modify its passive layer composition.

Chromium nitride (CrN) films, extensively applied in bearing spindles, stamping dies, cutting tools, and many other mechanical components due to excellent wear resistance, high ductility, toughness, and adhesion strength [195,196], have been widely investigated for PEMFC applications in recent years. CrN films are mainly produced by PVD [197,198] and arc ion plating (AIP) [199–201] methods. In addition, TiN films developed by PVD [202] and AIP [203,204] exhibited similar performance enhancement.

Carbon-based films, exhibiting good conduction performance due to a high fraction of C-sp^2 bonds, have drawn worldwide attention. Great attempts have been conducted to develop carbon based films using different approaches, including pure carbon film, chromium carbon (Cr-C) film, and titanium (Ti-C) carbon films. Fukutsuka et al. [205,206] produced a carbon layer on polished SS304 sheets with a thickness of 0.1 mm using a plasma-assisted chemical vapor deposition (CVD) method. Experimental results showed that the current density was less than 1 $\mu A/cm^2$ at 0.6 V vs. saturated calomel electrode (SCE) and the ICR was also greatly reduced. Factors affecting the formation of the carbon film were also investigated in detail [207]. Regarding Cr-C films, Hovsepian et al. [208] deposited a type of nanoscale multilayer structure in Cr-C coatings by the combined steered cathodic arc/unbalanced magnetron sputtering technique. A coating growth model was proposed to explain the phase separation and formation of the self-organized layered nanostructure observed in Cr-C coatings. Yi et al. [209] developed a multilayered Cr-C/a-C:Cr coating with the thickness of 1.4 μm on SS316L sheet by closed field unbalanced magnetron sputter ion plating (CFUBMSIP). ICR between the coated SS316L sheets and carbon paper was only 2.89 $m\Omega \cdot cm^2$ at 1.5 MPa.

6.2. Innovative Material and 3D Flow Field for Future Bipolar Plates

The performance of fuel cells is not only associated with physical-chemical and fluid-dynamic phenomenon, but also related to the flow field design of BPPs. High porosity carbons, carbon cloths, SS felts, and nickel foams were examined as alternatives to machined graphite gas flow fields [210]. Poorly designed flow fields can cause inefficient water removal and hinder reactant transport. Porous carbon foam was firstly proposed as the gas flow field in Maricle et al.'s study [211]. Kumar and Reddy used metal foams in the flow field of BPPs [212]. These fuel cells showed fair performance. Tang [213] designed a novel porous flow field made of the porous copper fiber sintered felt (PCFSF) and investigated the feasibility of this material, as shown in Figure 8. Experimental results revealed that a lower cutting speed helps prevent the fibers from failure during forming and morphological defects.

In Tseng's work [214], metal foams were used as flow distributors in the PEMFCs which outperformed the PEM fuel cells with conventional flow channels. Yuan et al. [215] reported that metal wire mesh was a new way to create porous structure. The structure was mostly determined by the wire diameter and number of layers, as well as the weaving method. The interlaced wires could be woven in different manners to achieve different pore shapes (e.g., circular, rectangular, polygonal, etc.) and mesh textures (e.g., horizontal, vertical and oblique, etc.). Likewise, the perforated metal plates may also have different hole-arrays and shapes, thereby yielding different opening patterns and ratios.

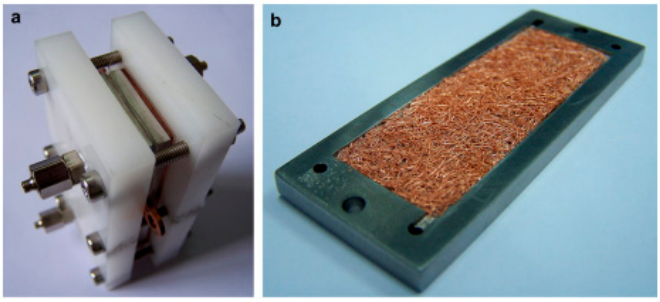

Figure 8. Schematic of the configuration of a PEMFC with a PCFSF flow field [213].

Recently, Toyota used a 3D fine-mesh flow field in the FCV MIRAI. Due to the increase of reaction gas turbulence, a uniform gas concentration gradient was obtained by the flow field. For a conventional straight channel, the generated water can accumulate easily within the cells, inhibiting electricity generation. The 3D fine-mesh flow field provides an even supply of air into the surface of the cells, while smoothly expelling the water resulting from electricity generation, thereby preventing water accumulation.

7. Development of High-Durability Processing Technologies

For automobile applications, PEMFCs must operate under various conditions, such as load changing cycles, high power conditions, idling conditions, and startup/shutdown cycles. Frequent dynamic processes can affect the durability of fuel cell system, which has limited its large-scale commercialization [216–218]. Therefore, it is important and urgent to investigate the PEMFC dynamic processes and promote effective mitigation strategies [219–221].

7.1. Degradation Mechanism

7.1.1. Startup/Shutdown Processes

In recent years, significant research efforts have been focused on the degradation behaviors under startup and shutdown conditions. And it is believed that the major cause of performance degradation during those processes is the local gas mixture at the anode called hydrogen/air interface or fuel/air interface [221]. Before startup, both the anode and cathode are exposed to air. As soon as the hydrogen is fed into the anode channels (also shown in Figure 9 [221]), the $V^a{}_m$ is brought to equilibrium potential of hydrogen ($V^{eq}{}_{H2} \approx 0.0$ V) in region A, increasing the cell voltage to about 0.85 V. Due to the high electron conductivity of the anode catalyst layer, the air remaining in region B lowers the electrolyte potential Φ to reach the same $V^a{}_m$. As a result, the interfacial potential difference of the cathode side in region B becomes higher than $V^{eq}{}_{O2}$, 1.44 V or larger. This high cathode potential temporarily reverses the current where air is present in the anode, causing severe carbon oxidation (also shown in Figure 10 [222]). Furthermore, Shen et al. [223] developed a special fuel cell system with a reference hydrogen electrode to illustrate the influences of the hydrogen/air interface at the anode. The high interfacial potential difference between the cathode and membrane could be observed and the reverse current degradation mechanism was proven experimentally. Meanwhile, the same phenomenon was also recently observed and researched by Plug Power Inc. In addition, many researchers studied the influence of the operating parameters including humidity, cell temperature, flow rate, and flow field design on the degradation rate of PEMFCs [224–226].

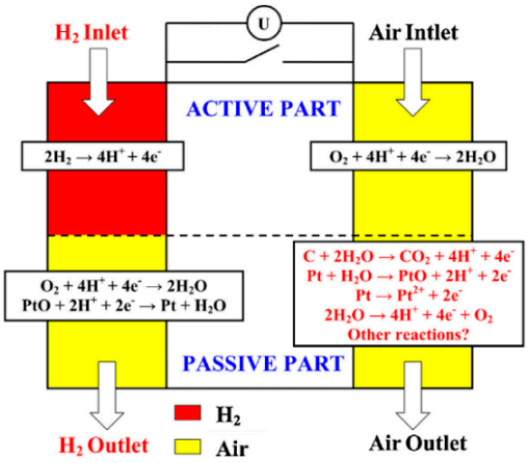

Figure 9. Reverse currents during startup [221].

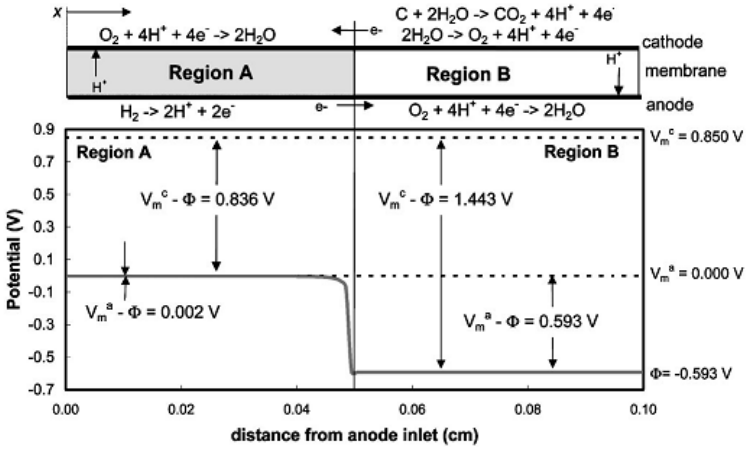

Figure 10. Potential distribution during reverse current conditions [222].

7.1.2. Load Variation Processes

In real operating conditions of vehicular application, fuel cells are always operating under variable load conditions. Frequent load changing leads to voltage fluctuations ranging from 0.4 V to 1.0 V (vs. RHE) [227]. During the load variation processes, the anode voltage is usually considered as 0 V due to the fast hydrogen oxidation reaction (HOR) rate and barely changes, while the cathode frequently fluctuates [221]. When a feedback system is used to control the load variation of PEMFCs, air starvation temporarily occurs due to the air supply rate lagging the loading rate [228]. Gas starvation leads to more drastic changes in the fuel cell voltage, and even causes cell reversal. Liang et al. [229] found water electrolysis would take place while cell reversal results in significant performance degradation. Meanwhile, the load variation process of PEMFCs is a very complex phenomenon, which is affected by many parameters, such as reactant stoichiometric ratio [216,230], reactant flow rate [231], loading range [220], loading speed [220], anode and cathode humidity [230–232], anode and cathode pressure [230] and proper reactant supply system [233].

Considering PEMFCs with a large active area, there is a spatial variation in the reactant and product concentrations along the channel length, which could lead to current, voltage, and temperature fluctuations. Moreover, reactant starvation worsens the situation [228]. A lot of studies of the distribution characteristics of fuel cells have been undertaken by researchers at Dalian institute of chemical physics (DICP). Yan et al. [234] investigated the current distribution and temperature distribution as well as their dynamic changes in the fuel cell stack. The results showed the temperature

of gas inlet could be higher than that of gas outlet during rapid loading. Furthermore, the voltage distribution was also evaluated during load changing. And the main reason of the voltage variation was found to be reaction gas starvation. Liang et al. [229] studied the fuel starvation phenomena in a single PEMFC. Experimental results showed that the current distribution is extremely uneven during the cell reversal process caused by fuel starvation. The HOR and water electrolysis could take place simultaneously in different regions at the anode, accelerating the corrosion of carbon support and degradation of membrane. All the uneven distribution described above can lead to rapid performance decay and shorter lifetime of PEMFCs.

7.2. Mitigation Strategies

7.2.1. Startup/Shutdown Processes

As discussed earlier, the formation of hydrogen/air interface during startup and shutdown is the primary reason for the degradation in PEMFC performance. The corresponding mitigation strategies mainly focus on two aspects: material improvements for stable catalyst supports and control strategies for conventional carbon-black catalyst supports.

Developing a more stable catalyst support to replace carbon-black has been one important mitigation strategy. The traditional catalyst support can be replaced by corrosion-resistant carbon materials or non-carbon materials. Yu et al. [235] used graphitized carbon as a catalyst support instead of a conventional support, and Owenjan et al. [236] also blended graphitized carbon in a microporous layer (MPL). Both studies reported the reduction in the PEMFC performance degradation. In addition to graphitized carbon, other carbon materials like carbon nanofibers and carbon nanotubes have also been considered. These materials have more stable electrochemical behavior than carbon-black. However, their synthesis costs are very high [237]. Another method is developing non-carbon supports such as titanium oxide [238], tungsten carbide [239] and indium tin oxide [240]. However, few studies have been found on PEMFC dynamic degradation using non-carbon catalyst support.

To avoid a hydrogen/air interface at the anode and eliminate the high potential at the cathode during dynamic operation, UTC, GM, Ford, Toyota, and other automotive companies have proposed many system strategies to mitigate dynamic degradation. These strategies can be classified into two major categories: gas purge and auxiliary load.

Gas purging is an effective and convenient strategy to prevent the formation of a hydrogen/air interface and reduce its residence time. It will displace the hydrogen/air with air, nitrogen, or other purge gas. For the startup process of PEMFCs, UTC Fuel Cells [241] presented a systemic strategy of gas purging. In their patent, hydrogen-rich air was used as purge gas in the cathode flow field. Their strategy could reduce the corrosion of carbon support. Toyota [242] combined hydrogen sensors and a gas purging system in the fuel cell during startup, preventing the formation of hydrogen/air interface. The Ford Motor Company [243] invented a gas separator, enriching nitrogen from exhaust gas in the stacks. The nitrogen-rich gas could purge the stacks to mitigate dynamic degradation. Also, GM [244] has proposed a similar gas purge strategy during startup/shutdown processes.

The residual gas in the flow field was removed easily by gas purging, but the gas remaining in the catalyst layer and gas diffusion layer could not be completely dispelled. Another effective method to remove the residual gas is to add a dummy load (also called auxiliary load). UTC Fuel Cells [245] proposed a strategy where an auxiliary load and anode exhaust recycle loop were combined and applies it to the startup process in fuel cells. The results showed that the performance loss with a dummy load was much lower than that without the dummy load. Shen et al. [223] also used a dummy load during the shutdown process. The results showed that this dummy load can reduce the performance degradation of fuel cells. Furthermore, electronic shorts of fuel cell can be applied as another way of using auxiliary loads. Ramani and Miller [246] employed electronic shorts for consuming the residual gas in the fuel cell, reducing the high potential occurring at the cathode. This strategy could be used during startup and shutdown process.

7.2.2. Mitigation Strategies during Load Variation Processes

As mentioned above, load changing and uneven distribution of PEMFCs can result in gas starvation, which in turn causes performance degradation. The effective methods to suppress gas starvation include improvement of the materials, algorithm controller, and gas storage.

Improving the electrode materials can achieve high flexibility under dynamic operation. The materials consist of an electrochemical catalyst, catalyst support, and PEM with high stability. Moreover, the supercapacitor material can be added in the cathode catalyst to improve the dynamic response characteristics. Wu et al. [247] prepared $RuO_2 \cdot xH_2O$/CNTs by the sol-gel method, which were sprayed onto the Pt/C electrode surface to form the cathode. It was found that the fuel cell had a better dynamic response performance with the composite cathode due to the capacity characteristics of $RuO_2 \cdot xH_2O$/CNTs.

He et al. and Ahn et al. [248] invented an air supply system including an integrator. This strategy ensured that the stoichiometry of the air was adapted for load changing. The voltage of the cells change with the load ranging, modifying the air supply. This strategy can promote the dynamic response of the fuel cell. Abdullah et al. [249] optimized the system control algorithm. Laguerre and exponential weight functions were proposed to mitigate oxygen starvation problems. The robustness and stability of the proposed controller were assessed using Monte-Carlo simulations.

UTC Fuel Cells [250] designed fuel flow channels at the end cell at the anode which were about 0.15 mm or 1.5 mm deeper than the remaining region. The space is designed to store hydrogen to avoid fuel starvation during a cold startup process. GM [251] has implemented a similar strategy, including a hydrogen source, an anode bleed valve, and a cell voltage monitor. If the controller detects a decrease in the minimum cell voltage, the sub-system will increase anode pressure by decreasing the molar faction of nitrogen. Meanwhile, recycling fuel gas is also a way to solve the fuel starvation problem. Yan et al. [252] at DICP also employed a feed forward control strategy and preset extra air storage. This strategy could mitigate the voltage fluctuation and extend the service time of the fuel cell.

8. Summary and Outlook

Through a decade of continuous global R&D, the performances of PEMFCs for vehicle application, such as energy efficiency, volumetric and mass specific power density, and low temperature startup ability have achieved significant breakthroughs. These technological achievements are closely related to the performance enhancement of the key materials and components for PEMFCs. The latest progress in proton exchange membranes, catalysts, catalyst layers, gas diffusion layers, and bipolar plates etc. have been reviewed and analyzed in this paper. For PEMs, the development direction is positioned in the preparation of composite and enhanced membranes with shorter side chains and lower EW values. The nanofiber enhanced multi-acid side chain membrane from 3M has shown high overall performance. For catalyst layers based on 3M's NSTF ordered catalyst layer, the 0.6V@2.0A/cm^2 MEA power generation performance can be attained under the ultra-low Pt loading of 0.14 g_{Pt}/kW. For the gas diffusion layer, the technical difficulties of water and air mass transfer have not been completely resolved; the performance of fuel cells at higher current density can be achieved through the development of novel GDLs with higher water and air mass transfer values. For bipolar plates, although the specific power density has been increased up to 5 kW/L, H_2 permeation still needs to be further enhanced. Regarding long-term durability, the dynamic operation is the main reason for the degradation of PEMFCs. Regardless of the startup and shutdown or load cycling processes, a very high potential will occur at the cathode, resulting in the loss of the catalyst and corrosion of the catalyst support. Among the various mitigation strategies, the primary methods are preventing the appearance of the hydrogen/air interface and avoiding gas starvation, moreover, the key materials properties improvement can also enhance the PEMFC durability under automobile operation conditions. The improvement of key materials in the stacks can enhance the dynamic response inside the cells.

The durability and cost of fuel cells for vehicle application have not yet met the targets of industrialization, where durability is considered to be the most important obstacle. In the future,

the novel R&D of key materials and components of fuel cells need to be considered in term of the degradation mechanisms and alleviation strategies under actual working conditions. The scale-up production techniques also need to be developed simultaneously so the gap between state-of-the-art and the targets can be minimized. Thus, the targets of cost and durability properties can be achieved.

Acknowledgments: This work is financially supported by National Science Foundation of China (NSFC) (Grant Nos. U1462112, 21573122, 51372271), Ministry of Science and Technology of China (Grand No. 2016YFB0101200), National Key Basic Research Program of China (Grant Nos. 2012CB215401, 2012CB215402) and the Program of International ST Cooperation (Grant Nos. 2013DFG41460, 2013DFG60080).

Author Contributions: Cheng Wang organized the paper; Shubo Wang wrote the second section "Proton Exchange Membranes"; Junliang Zhang wrote the third section "Catalysts System"; Jun Huang wrote the fourth section "Catalyst Layer"; Cheng Wang wrote the fifth section "Gas Diffusion Layer"; Linfa Peng wrote the sixth section "Bipolar Plates"; Zhigang Shao wrote the seventh section "Development of High-Durability Processing Technologies"; Chunwen Sun, Minggao Ouyang and Xiangming He helped to analyze data.

Conflicts of Interest: The authors declare no conflict of interest.

References

1. Ouyang, M.G. Technology strategy and R & D progress of automotive new energy and powertrain. *Trans. CSICE* **2008**, *26*, 107–114.
2. Sung, W.; Song, Y.; Yu, K.; Lim, T. Recent Advances in the Development of Hyundai·Kia's Fuel Cell Electric Vehicles. *SAE Int. J. Engines* **2010**, *3*, 768–772.
3. Wang, C.; Wang, S.B.; Zhang, J.B.; Li, J.Q.; Wang, J.L.; Ouyang, M.G. The Durability Research on the Proton Exchange Membrane Fuel Cell for Automobile Application. *Prog. Chem.* **2015**, *27*, 424–435.
4. Li, J.Q.; Fang, C.; Xu, L.F. Current status and trends of the research and development for fuel cell vehicles. *J. Automot. Saf. Energy* **2014**, *5*, 17–29.
5. Jones, D.J.; Change, G. *Energy Issues and Regulation Policies*; Springer: Dordrecht, The Netherlands, 2013; Volume 161.
6. The Fuel Cell Technical Team. *Fuel Cell Technical Team Roadmap*; DOE: Washington, DC, USA, 2013.
7. Mench, M. *Polymer Electrolyte Fuel Cell Degradation*; Elsevier: Amsterdam, The Netherlands, 2011; Volume 112.
8. Holmström, N.; Wiezell, K.; Lindbergh, G. Studying low-humidity effects in PEFCs using EIS: I. Experimental fuel cells, electrolyzers, and energy conversion. *J. Electrochem. Soc.* **2012**, *159*, F369–F378.
9. Makharia, R.; Kocha, S.S.; Yu, P.T.; Sweikart, M.A.; Gu, W.; Wagner, F.T.; Gasteiger, H.A. Durable PEM fuel cell electrode materials: Requirements and benchmarking methodologies. *ECS Trans.* **2006**, *1*, 3–18.
10. Hooshyari, K.; Javanbakht, M.; Shabanikia, A.; Enhessari, M. Fabrication $BaZrO_3$/PBI-based nanocomposite as a new proton conducting membrane for high temperature proton exchange membrane fuel cells. *J. Power Sources* **2015**, *276*, 62–72.
11. Rosero-Navarro, N.C.; Domingues, E.M.; Sousa, N.; Ferreira, P.; Figueiredo, F.M. Protonic conductivity and viscoelastic behaviour of Nafion membranes with periodic mesoporous organosilica fillers. *Int. J. Hydrog. Energy* **2014**, *39*, 5338–5349.
12. Singha, S.; Jana, T. Structure and properties of polybenzimidazole silica nanocomposite electrolyte membrane influence of organic inorganic interface. *ACS Appl. Mater. Interfaces* **2014**, *6*, 21286–21296.
13. Tominaga, Y.; Maki, T. Proton-conducting composite membranes based on polybenzimidazole and sulfonated mesoporous organosilicate. *Int. J. Hydrog. Energy* **2014**, *39*, 2724–2730.
14. Guo, Z.; Xu, X.; Xiang, Y.; Lu, S.; Jiang, S.P. New anhydrous proton exchange membranes for high-temperature fuel cells based on PVDF-PVP blended polymers. *J. Mater. Chem. A* **2015**, *3*, 148–155.
15. Perry, K.A.; More, K.L.; Payzant, E.A.; Meisner, R.A.; Sumpter, B.G.; Benicewicz, B.C. Comparative study of phosphoric acid-doped m-PBI membranes. *J. Polym. Sci. B Polym. Phys.* **2014**, *52*, 26–35.
16. Yuan, S.; Tang, Q.; He, B.; Chen, H.; Li, Q.; Ma, C.; Jin, S.; Liu, Z. H_3PO_4 imbibed polyacrylamide-graft-chitosan frameworks for high-temperature proton exchange membranes. *J. Power Sources* **2014**, *249*, 277–284.
17. Qin, Q.; Tang, Q.; Li, Q.; He, B.; Chen, H.; Wang, X.; Yang, P. Incorporation of H_3PO_4 into three-dimensional polyacrylamide-graft-starch hydrogel frameworks for robust high-temperature proton exchange membrane fuel cells. *Int. J. Hydrog. Energy* **2014**, *39*, 4447–4458.

18. Park, J.; Wang, L.; Advani, S.G.; Prasad, A.K. Mechanical stability of H_3PO_4-doped PBI hydrophilic-pretreated PTFE membranes for high temperature PEMFCs. *Electrochim. Acta* **2014**, *120*, 30–38.
19. Yang, J.S.; Cleemann, L.N.; Steenberg, T.; Terkelsen, C.; Li, Q.F.; Jensen, J.O.; Hjuler, H.A.; J. Bjerrum, N.; He, R.H. High molecular weight polybenzimidazole membranes for high temperature PEMFC. *Fuel Cells* **2014**, *14*, 7–15.
20. Jeon, Y.; Hwang, H.; Park, J.; Hwang, H.; Shul, Y. Temperature-dependent performance of the polymer electrolyte membrane fuel cell using short-side-chain perfluorosulfonic acid ionomer. *Int. J. Hydrog. Energy* **2014**, *39*, 11690–11699.
21. Zhang, H.; Li, J.; Tang, H.; Lin, Y.; Pan, M. Hydrogen crossover through perfluorosulfonic acid membranes with variable side chains and its influence in fuel cell lifetime. *Int. J. Hydrog. Energy* **2014**, *39*, 15989–15995.
22. Del Río, C.; Morales, E.; Escribano, P.G. Nafion sPOSS hybrid membranes for PEMFC Single cell performance and electrochemical characterization at different humidity conditions. *Int. J. Hydrog. Energy* **2014**, *39*, 5326–5337.
23. He, X.H.; Zheng, Y.; Yao, H.L.; Chen, Y.W.; Chen, D.F. Hybrid network sulfonated polynorbornene/silica membranes with enhanced proton conductivity by doped phosphotungstic acid. *Fuel Cells* **2014**, *14*, 26–34.
24. Bose, A.B.; Gopu, S.; Li, W. Enhancement of proton exchange membrane fuel cells performance at elevated temperatures and lower humidities by incorporating immobilized phosphotungstic acid in electrodes. *J. Power Sources* **2014**, *263*, 217–222.
25. Inagaki, S.; Guan, S.; Ohsuna, T.; Terasaki, O. An ordered mesoporous organosilica hybrid material with a crystal-like wall structure. *Nature* **2002**, *416*, 304–307.
26. Yang, Q.; Kapoor, M.P.; Inagaki, S. Sulfuric acid-functionalized mesoporous benzene-silica with a molecular-scale periodicity in the walls. *J. Am. Chem. Soc.* **2002**, *124*, 9694–9695.
27. Sharifi, M.; Kohler, C.; Tolle, P.; Frauenheim, T.; Wark, M. Proton conductivity of SO_3H-functionalized benzene-periodic mesoporous organosilica. *Small* **2011**, *7*, 1086–1097.
28. Domingues, E.M.; Salvador, M.A.; Ferreira, P.; Figueiredo, F.M. Acid-functionalised periodic mesoporous benzenosilica proton conductors. *Solid State Ion.* **2012**, *225*, 308–311.
29. Zhao, Z.; Pu, H.; Chang, Z.; Pan, H. A versatile strategy towards semi-interpenetrating polymer network for proton exchange membranes. *Int. J. Hydrog. Energy* **2014**, *39*, 6657–6663.
30. Li, H.Y.; Liu, Y.L. Nafion-functionalized electrospun poly vinylidene fluoride PVDF nanofibers for high performance proton exchange membranes in fuel cells. *J. Mater. Chem. A* **2014**, *2*, 3783–3793.
31. Moukheiber, E.; Bas, C.; Flandin, L. Understanding the formation of pinholes in PFSA membranes with the essential work of fracture (EWF). *Int. J. Hydrog. Energy* **2014**, *39*, 2717–2723.
32. Xiao, P.; Li, J.; Chen, R.; Wang, R.; Pan, M.; Tang, H. Understanding of temperature-dependent performance of short-side-chain perfluorosulfonic acid electrolyte and reinforced composite membrane. *Int. J. Hydrog. Energy* **2014**, *39*, 15948–15955.
33. D'Urso, C.; Oldani, C.; Baglio, V.; Merlo, L.; Arico, A.S. Towards fuel cell membranes with improved lifetime: Aquivion® Perfluorosulfonic Acid membranes containing immobilized radical scavengers. *J. Power Sources* **2014**, *272*, 753–758.
34. Kim, T.E.; Juon, S.M.; Park, J.H.; Shul, Y.G.; Cho, K.Y. Silicon carbide fiber-reinforced composite membrane for high-temperature and low-humidity polymer exchange membrane fuel cells. *Int. J. Hydrog. Energy* **2014**, *39*, 16474–16485.
35. Wang, L.; Advani, S.G.; Prasad, A.K. Self-hydrating Pt CeO_2-nafion composite membrane for improved durability and performance. *ECS Electrochem. Lett.* **2014**, *3*, F30–F32.
36. Wang, R.; Zhang, W.; He, G.; Gao, P. Controlling fuel crossover and hydration in ultra-thin proton exchange membrane-based fuel cells using Pt-nanosheet catalysts. *J. Mater. Chem. A* **2014**, *2*, 16416–16423.
37. Wang, R.J.; Yan, X.M.; Wu, X.M.; He, G.H.; Lin, D.; Hu, Z.W.; Tan, M. Modification of hydrophilic channels in Nafion membranes by DMBA mechanism and effects on proton conductivity. *J. Polym. Sci. B Polym. Phys.* **2014**, *52*, 1107–1117.
38. Napoli, L.; Franco, J.; Fasoli, H.; Sanguinetti, A. Conductivity of Nafion (R) 117 membrane used in polymer electrolyte fuel cells. *Int. J. Hydrog. Energy* **2014**, *39*, 8656–8660.
39. Li, G.; Xie, J.; Cai, H.; Qiao, J. New highly proton-conducting membrane based on sulfonated poly (arylene ether sulfone)s containing fluorophenyl pendant groups, for low-temperature polymer electrolyte membrane fuel cells. *Int. J. Hydrog. Energy* **2014**, *39*, 2639–2648.

40. Kwon, Y.; Lee, S.Y.; Hong, S.; Jang, J.H.; Henkensmeier, D.; Yoo, S.J.; Kim, H.J.; Kim, S.H. Novel sulfonated poly(arylene ether sulfone) containing hydroxyl groups for enhanced proton exchange membrane properties. *Polym. Chem.* **2015**, *6*, 233–239.
41. Wang, R.; Wu, X.; Yan, X.; He, G.; Hu, Z. Proton conductivity enhancement of SPEEK membrane through n-BuOH. *J. Membr. Sci.* **2015**, *479*, 46–54.
42. Seden, M.G.; Bastürk, E.; Inan, T.Y.; Apohan, N.K.; Güngor, A. Synthesis and fuel cell characterization of blend membranes from phenyl phosphine oxide containing flourinated novel polymers. *J. Power Sources* **2014**, *271*, 465–479.
43. Jetsrisuparb, K.; Balog, S.; Bas, C.; Perrin, L.; Wokaun, A.; Gubler, L. Proton conducting membranes prepared by radiation grafting of styrene and various comonomers. *Eur. Polym. J.* **2014**, *53*, 75–89.
44. He, Y.; Tong, C.; Geng, L.; Liu, L.; Lü, C. Enhanced performance of the sulfonated polyimide proton exchange membranes by graphene oxide Size effect of graphene oxide. *J. Membr. Sci.* **2014**, *458*, 36–46.
45. Armand, M.; Endres, F.; MacFarlane, D.R.; Ohno, H.; Scrosati, B. Ionic-liquid materials for the electrochemical challenges of the future. *Nat. Mater.* **2009**, *8*, 621–629. [PubMed]
46. Ye, H.; Huang, J.; Xu, J.J.; Kodiweera, N.K.A.C.; Jayakody, J.R.P.; Greenbaum, S.G. New membranes based on ionic liquids for PEM fuel cells at elevated temperatures. *J. Power Sources* **2008**, *178*, 651–660. [CrossRef]
47. Díaz, M.; Ortiz, A.; Ortiz, I. Progress in the use of ionic liquids as electrolyte membranes in fuel cells. *J. Membr. Sci.* **2014**, *469*, 379–396. [CrossRef]
48. Lemus, J.; Eguizábal, A.; Pina, M.P. Endurance strategies for the preparation of high temperature polymer electrolyte membranes by UV polymerization of 1-H-3-vinylimidazolium bis (trifluoromethanesulfonyl) imide for fuel cell applications. *Int. J. Hydrog. Energy* **2016**, *41*, 3981–3993. [CrossRef]
49. Jin, H.; O'Hare, B.; Dong, J.; Arzhantsev, S.; Baker, G.A.; Wishart, J.F. Physical properties of ionic liquids consisting of the 1-butyl-3-methylimidazolium cation with various anions and the bis(trifluoromethylsulfonyl)imide anion with various cations. *J. Phys. Chem. B.* **2007**, *112*, 81–92. [CrossRef] [PubMed]
50. Nieto de Castro, C.A.; Lourenço, M.J.V.; Ribeiro, A.P.C.; Langa, E.; Vieira, S.I.C.; Goodrich, P. Thermal Properties of Ionic Liquids and IoNanofluids of Imidazolium and Pyrrolidinium Liquids. *J. Chem. Eng. Data.* **2009**, *55*, 653–561. [CrossRef]
51. Ohno, H. Functional design of ionic liquids. *Bull. Chem. Soc. Jpn.* **2006**, *79*, 1665–1680. [CrossRef]
52. Olivier-Bourbigou, H.; Magna, L.; Morvan, D. Ionic liquids and catalysis: Recent progress from knowledge to applications. *Appl. Catal. A Gen.* **2010**, *373*, 1–56. [CrossRef]
53. Yandrasits, M. Fuel Cell Technical Team Roadmap. Available online: http://www.hydrogen.energy.gov/pdfs/review14/fc109_yandrasits_2014_o.pdf (accessed on 17 June 2014).
54. Aricò, A.S.; Blasi, A.D.; Brunaccini, G.; Sergi, F.; Dispenza, G.; Andaloro, L.; Ferraro, M.; Antonucci, V.; Asher, P.; Buche, S.; et al. High temperature operation of a solid polymer electrolyte fuel cell stack based on a new ionomer membrane. *Fuel Cells* **2010**, *10*, 1013–1023. [CrossRef]
55. Chen, C.; Kang, Y.; Huo, Z.; Zhu, Z.; Huang, W.; Xin, H.L.; Snyder, J.D.; Li, D.; Herron, J.A.; Mavrikakis, M. Highly crystalline multimetallic nanoframes with three-dimensional electrocatalytic surfaces. *Science* **2014**, *343*, 1339–1343. [CrossRef] [PubMed]
56. Cui, C.; Gan, L.; Li, H.H.; Yu, S.H.; Heggen, M.; Strasser, P. Octahedral PtNi nanoparticle catalysts: Exceptional oxygen reduction activity by tuning the alloy particle surface composition. *Nano Lett.* **2012**, *12*, 5885–5889. [CrossRef] [PubMed]
57. Huang, K.; Sasaki, K.; Adzic, R.R.; Xing, Y. Increasing Pt oxygen reduction reaction activity and durability with a carbon-doped TiO_2 nanocoating catalyst support. *J. Mater. Chem.* **2012**, *22*, 16824–16832. [CrossRef]
58. Guilminot, E.; Corcella, A.; Chatenet, M.; Maillard, F.; Charlot, F.; Berthomé, G.; Iojoiu, C.; Sanchez, J.Y.; Rossinot, E.; Claude, E. Membrane and active layer degradation upon PEMFC steady-state operation: I. Platinum dissolution and redistribution within the MEA fuel cells and energy conversion. *J. Electrochem. Soc.* **2007**, *154*, B1106–B1114. [CrossRef]
59. Meyers, J.P.; Darling, R.M. Model of carbon corrosion in PEM fuel cells batteries, fuel cells, and energy conversion. *J. Electrochem. Soc.* **2006**, *153*, A1432–A1442. [CrossRef]
60. Han, B.H.; Carlton, C.E.; Kongkanand, A.; Kukreja, R.S.; Theobald, B.R.; Gan, L.; O'Malley, R.; Strasser, P.; Wagner, F.T.; Shao-Horn, Y. Record activity and stability of dealloyed bimetallic catalysts for proton exchange membrane fuel cells. *Energy Environ. Sci.* **2015**, *8*, 258–266. [CrossRef]

61. Stamenkovic, V.R.; Fowler, B.; Mun, B.S.; Wang, G.; Ross, P.N.; Lucas, C.A.; Marković, N.M. Improved oxygen reduction activity on Pt3Ni(111) via increased surface site availability. *Science* **2007**, *315*, 493–497. [CrossRef] [PubMed]
62. Zhang, J.; Mo, Y.; Vukmirovic, M.; Klie, R.; Sasaki, K.; Adzic, R. Platinum monolayer electrocatalysts for O_2 reduction: Pt monolayer on Pd(111) and on carbon-supported Pd nanoparticles. *J. Phys. Chem. B* **2004**, *108*, 10955–10964. [CrossRef]
63. Zhang, J.; Vukmirovic, M.B.; Xu, Y.; Mavrikakis, M.; Adzic, R.R. Controlling the catalytic activity of platinum-monolayer electrocatalysts for oxygen reduction with different substrates. *Angew. Chem. Int. Ed.* **2005**, *44*, 2132–2135. [CrossRef] [PubMed]
64. Wang, J.X.; Inada, H.; Wu, L.J.; Zhu, Y.M.; Choi, Y.M.; Liu, P.; Zhou, W.P.; Adzic, R.R. Oxygen reduction on well-defined core-shell nanocatalysts: Particle size, facet, and Pt shell thickness effects. *J. Am. Chem. Soc.* **2009**, *131*, 17298–17302. [CrossRef] [PubMed]
65. Kuttiyiel, K.A.; Sasaki, K.; Choi, Y.; Su, D.; Liu, P.; Adzic, R.R. Nitride stabilized PtNi core-shell nanocatalyst for high oxygen reduction activity. *Nano Lett.* **2012**, *12*, 6266–6271. [CrossRef] [PubMed]
66. Adzic, R.; Wang, J.; Vukmirovic, M.; Sasaki, K.; Yang, S.H.; Malley, R.O. *Contiguous Platinum Monolayer Oxygen Reduction Electrocatalysts on High-Stability-Low-Cost Supports*; Hydrogen and Fuel Cells Program; DOE: Washington, DC, USA, 2010; pp. V26–V30.
67. Garsuch, A.; Stevens, D.A.; Sanderson, R.J.; Wang, S.; Atanasoski, R.T.; Hendricks, S.; Debe, M.K.; Dahn, J.R. Alternative Catalyst Supports Deposited on Nanostructured Thin Films for Proton Exchange Membrane Fuel Cells. *J. Electrochem. Soc.* **2010**, *157*, B187–B194. [CrossRef]
68. Bonakdarpour, A.; Stevens, K.; Vernstrom, G.D.; Atanasoski, R.; Schmoeckel, A.K.; Debe, M.K.; Dahn, J.R. Oxygen reduction activity of Pt and Pt-Mn-Co electrocatalysts sputtered on nano-structured thin film support. *Electrochim. Acta* **2007**, *53*, 688–694. [CrossRef]
69. Debe, M.K. Advanced cathode catalysts and supports for PEM fuel cells. In Proceedings of the 2011 Hydrogen Program Annual Merit Review and Peer Evaluation Meeting, Washington, DC, USA, 9–13 May.
70. Debe, M.K.; Steinbach, A.; Atanasoski, R.; Vernstrom, G.; Hendricks, S.; Kurkowski, M.; Hester, A.; Larson, J. Advanced cathode catalysts and supports for PEM fuel cells. In Proceedings of the 2010 Hydrogen Program Annual Merit Review and Peer Evaluation Meeting, Washington, DC, USA, 7–11 June 2010.
71. Zelenay, P. Non-Precious Metal Fuel Cell Cathodes: Catalyst Development and Electrode Structure Design. Available online: https://www.hydrogen.energy.gov/pdfs/review13/fc107_zelenay_2013_p.pdf (accessed on 13 May 2013).
72. Serov, A.; Artyushkova, K.; Atanassov, P. Fe-N-C oxygen reduction fuel cell catalyst derived from carbendazim: Synthesis, structure, and reactivity. *Adv. Energy Mater.* **2014**, *4*, 919–926. [CrossRef]
73. Zhou, Y.; Neyerlin, K.; Olson, T.S.; Pylypenko, S.; Bult, J.; Dinh, H.N.; Gennett, T.; Shao, Z.; O'Hayre, R. Enhancement of Pt and Pt-alloy fuel cell catalyst activity and durability via nitrogen-modified carbon supports. *Energy Environ. Sci.* **2010**, *3*, 1437–1446. [CrossRef]
74. Zhang, C.; Xu, L.; Shan, N.; Sun, T.; Chen, J.; Yan, Y. enhanced electrocatalytic activity and durability of Pt particles supported on ordered mesoporous carbon spheres. *ACS Catal.* **2014**, *4*, 1926–1930. [CrossRef]
75. Hsu, C.H.; Wu, H.M.; Kuo, P.L. Excellent performance of Pt on high nitrogen-containing carbon nanotubes using aniline as nitrogen/carbon source, dispersant and stabilizer. *Chem. Commun.* **2010**, *46*, 7628–7630. [CrossRef] [PubMed]
76. Seselj, N.; Engelbrekt, C.; Zhang, J. Graphene-supported platinum catalysts for fuel cells. *Sci. Bull.* **2015**, *60*, 864–876. [CrossRef]
77. Cheng, K.; He, D.P.; Peng, T.; Lv, H.F.; Pan, M.; Mu, S.C. Porous graphene supported Pt catalysts for proton exchange membrane fuel cells. *Electrochim. Acta* **2014**, *132*, 356–363. [CrossRef]
78. Sun, Q.; Kim, S. Synthesis of nitrogen-doped graphene supported Pt nanoparticles catalysts and their catalytic activity for fuel cells. *Electrochim. Acta* **2015**, *153*, 566–573. [CrossRef]
79. Jafri, R.I.; Rajalakshmi, N.; Dhathathreyan, K.S.; Ramaprabhu, S. Nitrogen doped graphene prepared by hydrothermal and thermal solid state methods as catalyst supports for fuel cell. *Int. J. Hydrog. Energy* **2015**, *40*, 4337–4348. [CrossRef]
80. Lei, M.; Wang, Z.B.; Li, J.S.; Tang, H.L.; Liu, W.J.; Wang, Y.G. CeO_2 nanocubes-graphene oxide as durable and highly active catalyst support for proton exchange membrane fuel cell. *Sci. Rep.* **2013**, *4*, 7415–7415. [CrossRef] [PubMed]

81. Jiang, Z.Z.; Wang, Z.B.; Qu, W.L.; Gu, D.M.; Yin, G.P. Synthesis and characterization of carbon riveted Pt/MWCNTs@TiO2-TiC catalyst with high durability for PEMFCs application. *Appl. Catal. B Environ.* **2012**, *123–124*, 214–220. [CrossRef]
82. Ignaszak, A.; Song, C.J.; Zhu, W.M.; Zhang, J.J.; Bauer, A.; Baker, R.; Neburchilov, V.; Ye, S.Y.; Campbell, S. Titanium carbide and its core-shelled derivative TiC@TiO_2 as catalyst supports for proton exchange membrane fuel cells. *Electrochim. Acta* **2012**, *69*, 397–405. [CrossRef]
83. Zhao, Y.L.; Wang, Y.H.; Cheng, X.Z.; Dong, L.; Zhang, Y.; Zang, J.B. Platinum nanoparticles supported on epitaxial TiC/nanodiamond as an electrocatalyst with enhanced durability for fuel cells. *Carbon* **2014**, *67*, 409–416. [CrossRef]
84. Stamatin, S.N.; Speder, J.; Dhiman, R.; Arenz, M.; Skou, E.M. Electrochemical stability and postmortem studies of Pt/SiC catalysts for polymer electrolyte membrane fuel cells. *ACS Appl. Mater. Interfaces* **2015**, *7*, 6153–6161. [CrossRef] [PubMed]
85. Dong, L.; Zang, J.B.; Su, J.; Jia, Y.D.; Wang, Y.H.; Lu, J.; Xu, X.P. Oxidized carbon/nano-SiC supported platinum nanoparticles as highly stable electrocatalyst for oxygen reduction. *Int. J. Hydrog. Energy* **2014**, *39*, 16310–16317. [CrossRef]
86. Dhiman, R.; Stamatin, S.N.; Andersen, S.M.; Morgenb, P.; Skoua, E.M. Oxygen reduction and methanol oxidation behaviour of SiC based Pt nanocatalysts for proton exchange membrane fuel cells. *J. Mater. Chem. A* **2013**, *1*, 15509–15516. [CrossRef]
87. Liang, C.; Ding, L.; Li, C.; Pang, M.; Su, D.; Li, W.; Wang, Y. Nanostructured WCx/CNTs as highly efficient support of electrocatalysts with low Pt loading for oxygen reduction reaction. *Energy Environ. Sci.* **2010**, *3*, 1121–1127. [CrossRef]
88. Liu, Y.; Mustain, W.E. High stability, high activity Pt/ITO oxygen reduction electrocatalysts. *J. Am. Chem. Soc.* **2012**, *135*, 530–533. [CrossRef] [PubMed]
89. Nie, M.; Shen, P.K.; Wu, M.; Wei, Z.; Meng, H. A study of oxygen reduction on improved Pt-WC/C electrocatalysts. *J. Power Sources* **2006**, *162*, 173–176. [CrossRef]
90. Gasteiger, H.A.; Kocha, S.S.; Sompalli, B.; Wagner, F.T. Activity benchmarks and requirements for Pt, Pt-alloy, and non-Pt oxygen reduction catalysts for PEMFCs. *Appl. Catal. B Environ.* **2005**, *56*, 9–35. [CrossRef]
91. Mathias, M.F.; Makharia, R.; Gasteiger, H.A.; Conley, J.J.; Fuller, T.J.; Gittleman, C.J.; Kocha, S.S.; Miller, D.P.; Mittelsteadt, C.K.; Xie, T. Two fuel cell cars in every garage. *Electrochem. Soc. Interface* **2005**, *14*, 24–35.
92. Wagner, F.T.; Yan, S.G.; Yu, P.T. Catalyst and catalyst-support durability. In *Handbook of Fuel Cells*; EG&G Technical Services, Inc.: Morgantown, WV, USA, 2009.
93. Ishiguro, N.; Kityakarn, S.; Sekizawa, O.; Uruga, T.; Sasabe, T.; Nagasawa, K.; Yokoyama, T.; Tada, M. Rate enhancements in structural transformations of Pt-Co and Pt-Ni bimetallic cathode catalysts in polymer electrolyte fuel cells studied by in situ time-resolved X-ray absorption fine structure. *J. Phys. Chem. C* **2014**, *118*, 15874–15883. [CrossRef]
94. Ticianelli, E.A. Methods to advance technology of proton exchange membrane fuel cells electrochemical science and technology. *J. Electrochem. Soc.* **1988**, *135*, 2209–2214. [CrossRef]
95. Wilson, M.S.; Gottesfeld, S. Thin-film catalyst layers for polymer electrolyte fuel cell electrodes. *J. Appl. Electrochem.* **1992**, *22*, 1–7. [CrossRef]
96. Litster, S.; McLean, G. PEM fuel cell electrodes. *J. Power Sources* **2004**, *130*, 61–76. [CrossRef]
97. Shukla, S.; Domican, K.; Karan, K.; Bhattacharjee, S.; Secanell, M. Analysis of low platinum loading thin polymer electrolyte fuel cell electrodes prepared by inkjet printing. *Electrochim. Acta* **2015**, *156*, 289–300. [CrossRef]
98. Wang, X.; Richey, F.W.; Wujcik, K.H.; Elabd, Y.A. Ultra-low platinum loadings in polymer electrolyte membrane fuel cell electrodes fabricated via simultaneous electrospinning/electrospraying method. *J. Power Sources* **2014**, *264*, 42–48. [CrossRef]
99. Mróz, W.; Budner, B.; Tokarz, W.; Piela, P.; Korwin-Pawlowski, M.L. Ultra-low-loading pulsed-laser-deposited platinum catalyst films for polymer electrolyte membrane fuel cells. *J. Power Sources* **2015**, *273*, 885–893. [CrossRef]
100. Li, B.; Yan, Z.; Higgins, D.C.; Yang, D.; Chen, Z.; Ma, J. Carbon-supported Pt nanowire as novel cathode catalysts for proton exchange membrane fuel cells. *J. Power Sources* **2014**, *262*, 488–493. [CrossRef]

101. Martin, S.; Martinez-Vazquez, B.; Garcia-Ybarra, P.L.; Castillo, J.L. Peak utilization of catalyst with ultra-low Pt loaded PEM fuel cell electrodes prepared by the electrospray method. *J. Power Sources* **2013**, *229*, 179–184. [CrossRef]
102. Huang, T.; Shen, H.; Jao, T.; Weng, F.; Su, A. Ultra-low Pt loading for proton exchange membrane fuel cells by catalyst coating technique with ultrasonic spray coating machine. *Int. J. Hydrog. Energy* **2012**, *37*, 13872–13879. [CrossRef]
103. Millington, B.; Whipple, V.; Pollet, B.G. A novel method for preparing proton exchange membrane fuel cell electrodes by the ultrasonic-spray technique. *J. Power Sources* **2011**, *196*, 8500–8508. [CrossRef]
104. Hwang, D.S.; Park, C.H.; Yi, S.C.; Lee, Y.M. Optimal catalyst layer structure of polymer electrolyte membrane fuel cell. *Int. J. Hydrog. Energy* **2011**, *36*, 9876–9885. [CrossRef]
105. Saha, M.S.; Malevich, D.; Halliop, E.; Pharoah, J.G.; Peppley, B.A.; Karan, K. Electrochemical activity and catalyst utilization of low Pt and thickness controlled membrane electrode assemblies fuel cells and energy conversion. *J. Electrochem. Soc.* **2011**, *158*, B562–B567. [CrossRef]
106. Soboleva, T.; Zhao, X.; Malek, K.; Xie, Z.; Navessin, T.; Holdcroft, S. On the micro-, meso-, and macroporous structures of polymer electrolyte membrane fuel cell catalyst layers. *ACS Appl. Mater. Interfaces* **2010**, *2*, 375–384. [CrossRef] [PubMed]
107. Middelman, E. Improved PEM fuel cell electrodes by controlled self-assembly. *Fuel Cells Bull.* **2002**, *2002*, 9–12. [CrossRef]
108. Ahn, C.; Cheon, J.; Joo, S.; Kim, J. Effects of ionomer content on Pt catalyst/ordered mesoporous carbon support in polymer electrolyte membrane fuel cells. *J. Power Sources* **2013**, *222*, 477–482. [CrossRef]
109. Fujigaya, T.; Nakashima, N. Fuel cell electrocatalyst using polybenzimidazole-modified carbon nanotubes as support materials. *Adv. Mater.* **2013**, *25*, 1666–1681. [CrossRef] [PubMed]
110. Kim, O.; Cho, Y.; Kang, S.H.; Park, H.; Kim, M.; Lim, J.W.; Chung, D.Y.; Lee, M.J.; Choe, H.; Sung, Y. Ordered macroporous platinum electrode and enhanced mass transfer in fuel cells using inverse opal structure. *Nat. Commun.* **2013**, *4*, 2473. [CrossRef] [PubMed]
111. Zeng, J.; Francia, C.; Dumitrescu, M.A.; Monteverde, V.A.H.A.; Ijeri, V.S.; Specchia, S.; Spinelli, P. Electrochemical performance of Pt-based catalysts supported on different ordered mesoporous carbons (Pt/OMCs) for oxygen reduction reaction. *Ind. Eng. Chem. Res.* **2012**, *51*, 7500–7509. [CrossRef]
112. Wang, T.; Zhang, C.; Sun, X.; Guo, Y.; Guo, H.; Tang, J.; Xue, H.; Liu, M.; Zhang, X.; Zhu, L.; Xie, Q.; He, J. Synthesis of ordered mesoporous boron-containing carbon films and their corrosion behavior in simulated proton exchange membrane fuel cells environment. *J. Power Sources* **2012**, *212*, 1–12. [CrossRef]
113. Tian, Z.Q.; Lim, S.H.; Poh, C.K.; Tang, Z.; Xia, Z.; Luo, Z.; Shen, P.K.; Chua, D.; Feng, Y.P.; Shen, Z.; Lin, J. A highly order-structured membrane electrode assembly with vertically aligned carbon nanotubes for ultra-low Pt loading PEM fuel cells. *Adv. Energy Mater.* **2011**, *1*, 1205–1214. [CrossRef]
114. Kim, J.H.; Fang, B.; Kim, M.; Yoon, S.B.; Bae, T.; Ranade, D.R.; Yu, J. Facile synthesis of bimodal porous silica and multimodal porous carbon as an anode catalyst support in proton exchange membrane fuel cell. *Electrochim. Acta* **2010**, *55*, 7628–7633. [CrossRef]
115. Dong, B.; Gwee, L.; Salas-de La Cruz, D.; Winey, K.I.; Elabd, Y.A. super proton conductive high-purity Nafion nanofibers. *Nano Lett.* **2010**, *10*, 3785–3790. [CrossRef] [PubMed]
116. Fang, B.; Kim, J.H.; Kim, M.; Yu, J. Ordered hierarchical nanostructured carbon as a highly efficient cathode catalyst support in proton exchange membrane fuel cell. *Chem. Mater.* **2009**, *21*, 789–796. [CrossRef]
117. Caillard, A.; Charles, C.; Boswell, R.; Brault, P. Improvement of the sputtered platinum utilization in proton exchange membrane fuel cells using plasma-based carbon nanofibers. *J. Phys. D Appl. Phys.* **2008**, *41*, 2824–2833. [CrossRef]
118. Pan, C.; Wu, H.; Wang, C.; Wang, B.; Zhang, L.; Cheng, Z.; Hu, P.; Pan, W.; Zhou, Z.; Yang, X.; et al. Nanowire-based high-performance "micro fuel cells": One nanowire, one fuel cell. *Adv. Mater.* **2008**, *20*, 1644–1648. [CrossRef]
119. Calvillo, L.; Lázaro, M.J.; García-Bordejé, E.; Moliner, R.; Cabot, P.L.; Esparbé, I.; Pastor, E.; Quintana, J.J. Platinum supported on functionalized ordered mesoporous carbon as electrocatalyst for direct methanol fuel cells. *J. Power Sources* **2007**, *169*, 59–64. [CrossRef]
120. Li, W.; Wang, X.; Chen, Z.; Waje, M.; Yan, Y. Carbon nanotube film by filtration as cathode catalyst support for proton-exchange membrane fuel cell. *Langmuir* **2005**, *21*, 9386–9389. [CrossRef] [PubMed]

121. Wang, C.; Waje, M.; Wang, X.; Tang, J.M.; Haddon, R.C.; Yan, Y. Proton exchange membrane fuel cells with carbon nanotube based electrodes. *Nano Lett.* **2004**, *4*, 345–348. [CrossRef]
122. Joo, S.H.; Choi, S.J.; Oh, I.; Kwak, J.; Liu, Z.; Terasaki, O.; Ryoo, R. Ordered nanoporous arrays of carbon supporting high dispersions of platinum nanoparticles. *Nature* **2001**, *412*, 169–172. [CrossRef] [PubMed]
123. Ryoo, R.; Joo, S.H.; Kruk, M.; Jaroniec, M. Ordered mesoporous carbons. *Adv. Mater.* **2001**, *13*, 677–681. [CrossRef]
124. Debe, M.K. Tutorial on the fundamental characteristics and practical properties of nanostructured thin film (NSTF) catalysts fuel cells, electrolyzers, and energy conversion. *J. Electrochem. Soc.* **2013**, *160*, F522–F534. [CrossRef]
125. Debe, M.K. Electrocatalyst approaches and challenges for automotive fuel cells. *Nature* **2012**, *486*, 43–51. [CrossRef] [PubMed]
126. Song, D.; Wang, Q.; Liu, Z.; Eikerling, M.; Xie, Z.; Navessin, T.; Holdcroft, S. A method for optimizing distributions of Nafion and Pt in cathode catalyst layers of PEM fuel cells. *Electrochim. Acta* **2005**, *50*, 3347–3358. [CrossRef]
127. Srinivasarao, M.; Bhattacharyya, D.; Rengaswamy, R.; Narasimhan, S. Performance analysis of a PEM fuel cell cathode with multiple catalyst layers. *Int. J. Hydrog. Energy* **2010**, *35*, 6356–6365. [CrossRef]
128. Matsuda, H.; Fushinobu, K.; Ohma, A.; Okazaki, K. Structural effect of cathode catalyst layer on the performance of PEFC. *J. Therm. Sci. Technol.* **2011**, *6*, 154–163. [CrossRef]
129. Roshandel, R.; Ahmadi, F. Effects of catalyst loading gradient in catalyst layers on performance of polymer electrolyte membrane fuel cells. *Renew. Energy* **2013**, *50*, 921–931. [CrossRef]
130. Fofana, D.; Hamelin, J.; Bénard, P. Modelling and experimental validation of high performance low platinum multilayer cathode for polymer electrolyte membrane fuel cells (PEMFCs). *Int. J. Hydrog. Energy* **2013**, *38*, 10050–10062. [CrossRef]
131. Fofana, D.; Natarajan, S.K.; Hamelin, J.; Benard, P. Low platinum, high limiting current density of the PEMFC (proton exchange membrane fuel cell) based on multilayer cathode catalyst approach. *Energy* **2014**, *64*, 398–403. [CrossRef]
132. Wilkinson, D.P.; St-Pierre, J. In-plane gradients in fuel cell structure and conditions for higher performance. *J. Power Sources* **2003**, *113*, 101–108. [CrossRef]
133. Prasanna, M.; Cho, E.A.; Kim, H.J.; Oh, I.H.; Lim, T.H.; Hong, S.A. Performance of proton-exchange membrane fuel cells using the catalyst-gradient electrode technique. *J. Power Sources* **2007**, *166*, 53–58. [CrossRef]
134. Cetinbas, F.C.; Advani, S.G.; Prasad, A.K. Investigation of a polymer electrolyte membrane fuel cell catalyst layer with bidirectionally-graded composition. *J. Power Sources* **2014**, *270*, 594–602. [CrossRef]
135. Lee, S.Y.; Kim, H.J.; Kim, K.H.; Cho, E.; Oh, I.H.; Lim, T.H. Gradient catalyst coating for a proton exchange membrane fuel cell operation under nonhumidified conditions. *Electrochem. Solid-State Lett.* **2007**, *10*, B166–B169. [CrossRef]
136. Cetinbas, F.C.; Advani, S.G.; Prasad, A.K. Optimization of polymer electrolyte membrane fuel cell catalyst layer with bidirectionally-graded composition. *Electrochim. Acta* **2015**, *174*, 787–798. [CrossRef]
137. Yuan, F.L.; Ryu, H.J. The synthesis, characterization, and performance of carbon nanotubes and carbon nanofibres with controlled size and morphology as a catalyst support material for a polymer electrolyte membrane fuel cell. *Nanotechnology* **2004**, *15*, S596–S602. [CrossRef]
138. Sinha, P.K.; Gu, W.; Kongkanand, A.; Thompson, E. Performance of nano structured thin film (NSTF) electrodes under partially-humidified conditions fuel cells and energy conversion. *J. Electrochem. Soc.* **2011**, *158*, B831–B840. [CrossRef]
139. Paulus, U.A.; Veziridis, Z.; Schnyder, B.; Kuhnke, M.; Scherer, G.G.; Wokaun, A. Fundamental investigation of catalyst utilization at the electrode/solid polymer electrolyte interface : Part I. Development of a model system. *J. Electroanal. Chem.* **2003**, *541*, 77–91. [CrossRef]
140. McBreen, J. Voltammetric studies of electrodes in contact with ionomeric membranes electrochemical science and technology—Technical papers. *J. Electrochem. Soc.* **1985**, *132*, 1112–1116. [CrossRef]
141. Chan, K.; Eikerling, M. Water balance model for polymer electrolyte fuel cells with ultrathin catalyst layers. *Phys. Chem. Chem. Phys.* **2013**, *16*, 2106–2117. [CrossRef] [PubMed]
142. Chan, K.; Eikerling, M. impedance model of oxygen reduction in water-flooded pores of ionomer-free PEFC catalyst layers. *J. Electrochem. Soc.* **2012**, *159*, B155–B164. [CrossRef]

143. Chan, K.; Eikerling, M. A pore-scale model of oxygen reduction in ionomer-free catalyst layers of PEFCs fuel cells and energy conversion. *J. Electrochem. Soc.* **2011**, *158*, B18–B28. [CrossRef]
144. Debe, M.K.; Atanasoski, R.T.; Steinbach, A.J. Nanostructured Thin Film Electrocatalysts—Current Status and Future Potential. In Proceedings of the 11th Polymer Electrolyte Fuel Cell Symposium (PEFC) Under the Auspices of the 220th Meeting of the ECS, Boston, MA, USA, October 2011.
145. El-Kharouf, A.; Rees, N.V.; Steinberger-Wilckens, R. Gas diffusion layer materials and their effect on polymer electrolyte fuel cell performance—Ex situ and in situ characterization. *Fuel Cells* **2014**, *14*, 735–741. [CrossRef]
146. Khajeh-Hosseini-Dalasm, N.; Sasabe, T.; Tokumasu, T.; Pasaogullari, U. Effects of polytetrafluoroethylene treatment and compression on gas diffusion layer microstructure using high-resolution X-ray computed tomography. *J. Power Sources* **2014**, *266*, 213–221. [CrossRef]
147. Cheema, T.A.; Kim, G.M.; Lee, C.Y.; Kwak, M.K.; Kim, H.B.; Park, C.W. Effects of composite porous gas-diffusion layers on performance of proton exchange membrane fuel cell. *Int. J. Precis. Eng. Manuf. Green Technol.* **2014**, *1*, 305–312. [CrossRef]
148. Lee, K.; Kang, J.H.; Nam, J.H. Liquid water distribution in hydrophobic gas-diffusion layers with interconnect rib geometry: An invasion-percolation pore network analysis. *Int. J. Hydrog. Energy* **2014**, *39*, 6646–6656. [CrossRef]
149. Mortazavi, M.; Tajiri, K. On the synthesis and characterization of silica-doped sulfonated poly-2,6-dimethyl-1,4-phenylene oxide composite membranes. *J. Fuel Cell Sci. Technol.* **2014**, *11*, 021002. [CrossRef]
150. Song, W.; Yu, H.; Shao, Z.; Yi, B.; Lin, J.; Liu, N. Effect of polytetrafluoroethylene distribution in the gas diffusion layer on water flooding in proton exchange membrane fuel cells. *Chin. J. Catal.* **2014**, *35*, 468–473. [CrossRef]
151. Mortazavi, M.; Tajiri, K. Effect of the PTFE content in the gas diffusion layer on water transport in polymer electrolyte fuel cells (PEFCs). *J. Power Sources* **2014**, *245*, 236–244. [CrossRef]
152. Kim, S.; Jeong, B.; Hong, B.K.; Kim, T.S. Effects of hydrophobic agent content in macro-porous substrates on the fracture behavior of the gas diffusion layer for proton exchange membrane fuel cells. *J. Power Sources* **2014**, *270*, 342–348. [CrossRef]
153. Koresawa, R.; Utaka, Y. Improvement of oxygen diffusion characteristic in gas diffusion layer with planar-distributed wettability for polymer electrolyte fuel cell. *J. Power Sources* **2014**, *271*, 16–24. [CrossRef]
154. Joo, J.; Choun, M.; Kim, K.; Uhm, S.; Kim, Y.D.; Lee, J. Controlled water flooding of polymer electrolyte fuel cells applying superhydrophobic gas diffusion layer. *Curr. Appl. Phys.* **2014**, *14*, 1374–1379. [CrossRef]
155. Latorrata, S.; Stampino, P.G.; Cristiani, C.; Dotelli, G. Novel superhydrophobic gas diffusion media for PEM fuel cells: Evaluation of performance and durability. *Chem. Eng. Trans.* **2014**, *41*, 241–246.
156. Gola, M.; Sansotera, M.; Navarrini, W.; Bianchi, C.L.; Stampino, P.G.; Latorrata, S.; Dotelli, G. Perfluoropolyether-functionalized gas diffusion layers for proton exchange membrane fuel cells. *J. Power Sources* **2014**, *258*, 351–355. [CrossRef]
157. Kitahara, T.; Nakajima, H.; Inamoto, M.; Shinto, K. Triple microporous layer coated gas diffusion layer for performance enhancement of polymer electrolyte fuel cells under both low and high humidity conditions. *J. Power Sources* **2014**, *248*, 1256–1263. [CrossRef]
158. Huang, G.; Chang, M. Effect of gas diffusion layer with double-side microporous layer coating on proton exchange membrane fuel cell performance under different air inlet relative humidity. *Int. J. Electrochem. Sci.* **2014**, *9*, 7819–7831.
159. Tanaka, S.; Shudo, T. Corrugated mesh flow channel and novel microporous layers for reducing flooding and resistance in gas diffusion layer-less polymer electrolyte fuel cells. *J. Power Sources* **2014**, *268*, 183–193. [CrossRef]
160. Choi, H.; Kim, O.; Kim, M.; Choe, H.; Cho, Y.; Sung, Y. Next-generation polymer-electrolyte-membrane fuel cells using titanium foam as gas diffusion layer. *ACS Appl. Mater. Interfaces* **2014**, *6*, 7665–7671. [CrossRef] [PubMed]
161. Fang, S.Y.; Huang, R.H.; Teoh, L.G.; Hsueh, K.L.; Chao, W.K.; Tsai, D.C.; Yang, T.N.; Shieu, F.S. Coating TiVCr hydrogen storage alloy on the anode gas diffusion layer of proton exchange membrane fuel cells to improve performance. *J. Power Sources* **2014**, *268*, 443–450. [CrossRef]
162. Dhakate, S.; Mathur, R.; Kakati, B.; Dhami, T. Properties of graphite-composite bipolar plate prepared by compression molding technique for PEM fuel cell. *Int. J. Hydrog. Energy* **2007**, *32*, 4537–4543. [CrossRef]

163. Wissler, M. Graphite and carbon powders for electrochemical applications. *J. Power Sources* **2006**, *156*, 142–150. [CrossRef]
164. Lee, S.J.; Hsu, C.D.; Huang, C.H. Analyses of the fuel cell stack assembly pressure. *J. Power Sources* **2005**, *145*, 353–361. [CrossRef]
165. Gregor, H. *Fuel Cell Technology Handbook*; CRC Press: New York, NY, USA, 2003.
166. Kang, S.J.; Kim, D.O.; Lee, J.H.; Lee, P.C.; Lee, M.H.; Lee, Y. Solvent-assisted graphite loading for highly conductive phenolic resin bipolar plates for proton exchange membrane fuel cells. *J. Power Sources* **2010**, *195*, 3794–3801. [CrossRef]
167. Dueramae, I.; Pengdam, A.; Rimdusit, S. *J. Appl. Polym. Sci.* **2013**, *130*, 3909–3918.
168. Oh, M.; Yoon, Y.; Park, S. The electrical and physical properties of alternative material bipolar plate for PEM fuel cell system. *Electrochim. Acta* **2004**, *50*, 777–780. [CrossRef]
169. Cho, E.; Jeon, U.S.; Ha, H.; Hong, S.A.; Oh, I.H. Characteristics of composite bipolar plates for polymer electrolyte membrane fuel cells. *J. Power Sources* **2004**, *125*, 178–182. [CrossRef]
170. Besmann, T.M.; Klett, J.W.; Henry, J.J.; Lara, C.E. Carbon/carbon composite bipolar plate for proton exchange membrane fuel cells. *J. Electrochem. Soc.* **2000**, *147*, 4083–4086. [CrossRef]
171. Cunningham, B.; Baird, D.G. The development of economical bipolar plates for fuel cells. *J. Mater. Chem.* **2006**, *16*, 4385–4388. [CrossRef]
172. Taherian, R.; Nasr, M. Performance and material selection of nanocomposite bipolar plate in proton exchange membrane fuel cells. *Int. J. Energy Res.* **2014**, *38*, 94–105. [CrossRef]
173. Kim, M.; Yu, H.N.; Lim, J.W.; Lee, D.G. Bipolar plates made of plain weave carbon/epoxy composite for proton exchange membrane fuel cell. *Int. J. Hydrog. Energy* **2012**, *37*, 4300–4308. [CrossRef]
174. Schmittinger, W.; Vahidi, A. A review of the main parameters influencing long-term performance and durability of PEM fuel cells. *J. Power Sources* **2008**, *180*, 1–14. [CrossRef]
175. Kuo, J.K.; Chen, C.K. A novel Nylon-6-S316L fiber compound material for injection molded PEM fuel cell bipolar plates. *J. Power Sources* **2006**, *162*, 207–214. [CrossRef]
176. Middelman, E.; Kout, W.; Vogelaar, B.; Lenssen, J.; de Waal, E. Bipolar plates for PEM fuel cells. *J. Power Sources* **2003**, *118*, 44–46. [CrossRef]
177. Karimi, S.; Fraser, N.; Roberts, B.; Foulkes, F.R. A review of metallic bipolar plates for proton exchange membrane fuel cells: Materials and fabrication methods. *Adv. Mater. Sci. Eng.* **2012**, *2012*, 1–22. [CrossRef]
178. Feng, K.; Wu, G.; Li, Z.; Cai, X.; Chu, P.K. Corrosion behavior of SS316L in simulated and accelerated PEMFC environments. *Int. J. Hydrog. Energy* **2011**, *36*, 13032–13042. [CrossRef]
179. Antunes, R.A.; Oliveira, M.C.L.; Ett, G.; Ett, V. Corrosion of metal bipolar plates for PEM fuel cells: A review. *Int. J. Hydrog. Energy* **2010**, *35*, 3632–3647. [CrossRef]
180. Hornung, R.; Kappelt, G. Bipolar plate materials development using Fe-based alloys for solid polymer fuel cells. *J. Power Sources* **1998**, *72*, 20–21. [CrossRef]
181. El-Enin, S.A.A.; Abdel-Salam, O.E.; El-Abd, H.; Amin, A.M. New electroplated aluminum bipolar plate for PEM fuel cell. *J. Power Sources* **2008**, *177*, 131–136. [CrossRef]
182. Joseph, S.; McClure, J.; Sebastian, P.; Moreira, J.; Valenzuela, E. Polyaniline and polypyrrole coatings on aluminum for PEM fuel cell bipolar plates. *J. Power Sources* **2008**, *177*, 161–166. [CrossRef]
183. Davies, D.P.; Adcock, P.L.; Turpin, M.; Rowen, S.J. Bipolar plate materials for solid polymer fuel cell. *J. Appl. Electrochem.* **2000**, *30*, 101–105. [CrossRef]
184. Zhang, H.; Hou, M.; Lin, G.; Han, Z.; Fu, Y.; Sun, S. Performance of Ti-Ag-deposited titanium bipolar plates in simulated unitized regenerative fuel cell (URFC) environment. *Int. J. Hydrog. Energy* **2011**, *36*, 5695–5701. [CrossRef]
185. Weil, K.S.; Kim, J.Y.; Xia, G.; Coleman, J.; Yang, Z.G. Boronization of nickel and nickel clad materials for potential use in polymer electrolyte membrane fuel cells. *Surf. Coat. Technol.* **2006**, *201*, 4436–4441. [CrossRef]
186. Paulauskas, I.E.; Brady, M.P.; Meyer, I.H.M.; Buchanan, R.A.; Walker, L.R. Corrosion behavior of CrN, Cr 2 N and π phase surfaces on nitrided Ni-50Cr for proton exchange membrane fuel cell bipolar plates. *Corros. Sci.* **2006**, *48*, 3157–3171. [CrossRef]
187. Nikam, V.V.; Reddy, R.G. Corrugated bipolar sheets as fuel distributors in PEMFC. *Int. J. Hydrog. Energy* **2006**, *31*, 1863–1873. [CrossRef]
188. Nikam, V.V.; Reddy, R.G. Copper alloy bipolar plates for polymer electrolyte membrane fuel cell. *Electrochim. Acta* **2006**, *51*, 6338–6345. [CrossRef]

189. Lee, S.J.; Huang, C.H.; Lai, J.J.; Chen, Y.P. Corrosion-resistant component for PEM fuel cells. *J. Power Sources* **2004**, *131*, 162–168. [CrossRef]
190. Lee, S.J.; Lai, J.J.; Huang, C.H. Stainless steel bipolar plates. *J. Power Sources* **2005**, *145*, 362–368. [CrossRef]
191. Cho, K.H.; Lee, W.G.; Lee, S.B.; Jang, H. Corrosion resistance of chromized 316L stainless steel for PEMFC bipolar plates. *J. Power Sources* **2008**, *178*, 671–676. [CrossRef]
192. Lee, S.B.; Cho, K.H.; Lee, W.G.; Jang, H. Improved corrosion resistance and interfacial contact resistance of 316L stainless-steel for proton exchange membrane fuel cell bipolar plates by chromizing surface treatment. *J. Power Sources* **2009**, *187*, 318–323. [CrossRef]
193. Feng, K.; Shen, Y.; Mai, J.; Liu, D.; Cai, X. An investigation into nickel implanted 316L stainless steel as a bipolar plate for PEM fuel cell. *J. Power Sources* **2008**, *182*, 145–152. [CrossRef]
194. Feng, K.; Shen, Y.; Liu, D.; Chu, P.K.; Cai, X. Ni-Cr Co-implanted 316L stainless steel as bipolar plate in polymer electrolyte membrane fuel cells. *Int. J. Hydrog. Energy* **2010**, *35*, 690–700. [CrossRef]
195. Vite, M.; Moreno-Ríos, M.; Hernández, E.A.G.; Laguna-Camacho, J.R. A study of the abrasive resistance of sputtered CrN coatings deposited on AISI 316 and AISI H13 steel substrates using steel particles. *Wear* **2011**, *271*, 1273–1279. [CrossRef]
196. Cho, C.W.; Lee, Y.Z. Wear-life evaluation of CrN-coated steels using acoustic emission signals. *Surf. Coat. Technol.* **2000**, *127*, 59–65. [CrossRef]
197. Barranco, J.; Barreras, F.; Lozano, A.; Maza, M. Influence of CrN-coating thickness on the corrosion resistance behaviour of aluminium-based bipolar plates. *J. Power Sources* **2011**, *196*, 4283–4289. [CrossRef]
198. Lavigne, O.; Alemany-Dumont, C.; Normand, B.; Berthon-Fabry, S.; Metkemeijer, R. Thin chromium nitride PVD coatings on stainless steel for conductive component as bipolar plates of PEM fuel cells: Ex-situ and in-situ performances evaluation. *Int. J. Hydrog. Energy* **2012**, *37*, 10789–10797. [CrossRef]
199. Fu, Y.; Lin, G.Q.; Hou, M.; Wu, B.; Li, H.K.; Hao, L.X. Optimized Cr-nitride film on 316L stainless steel as proton exchange membrane fuel cell bipolar plate. *Int. J. Hydrog. Energy* **2009**, *34*, 453–458. [CrossRef]
200. Wu, B.; Fu, Y.; Xu, J.; Lin, G.Q.; Hou, M. Chromium nitride films on stainless steel as bipolar plate for proton exchange membrane fuel cell. *J. Power Sources* **2009**, *194*, 976–980. [CrossRef]
201. Zhang, M.; Lin, G.Q.; Wu, B.; Shao, Z.G. Composition optimization of arc ion plated CrNx films on 316L stainless steel as bipolar plates for polymer electrolyte membrane fuel cells. *J. Power Sources* **2012**, *205*, 318–323. [CrossRef]
202. Wang, Y.; Northwood, D.O. An investigation of the electrochemical properties of PVD TiN-coated SS410 in simulated PEM fuel cell environments. *Int. J. Hydrog. Energy* **2007**, *32*, 895–902. [CrossRef]
203. Tian, R.J.; Sun, J.C. Corrosion resistance and interfacial contact resistance of TiN coated 316L bipolar plates for proton exchange membrane fuel cell. *Int. J. Hydrog. Energy* **2011**, *36*, 6788–6794. [CrossRef]
204. Zhang, D.M.; Duan, L.T.; Guo, L.; Tuan, W.H. Corrosion behavior of TiN-coated stainless steel as bipolar plate for proton exchange membrane fuel cell. *Int. J. Hydrog. Energy* **2010**, *35*, 3721–3726. [CrossRef]
205. Fukutsuka, T.; Yamaguchi, T.; Miyano, S.I.; Matsuo, Y.; Sugie, Y.; Ogumi, Z. Carbon-coated stainless steel as PEFC bipolar plate material. *J. Power Sources* **2007**, *174*, 199–205. [CrossRef]
206. Fukutsuka, T.; Yamaguchi, T.; Matsuo, Y.; Sugie, Y.; Ogumi, Z. Improvement in corrosion properties of carbon-coated Fe-based metals for PEFC bipolar plate. *Electrochemistry* **2007**, *75*, 152–154. [CrossRef]
207. Matsuo, Y.; Miyano, S.; Sugie, Y.; Fukutsuka, T. Factors affecting the formation of carbon film on the stainless steels for the bipolar plate of polymer electrolyte fuel cells. *J. Fuel Cell. Sci. Technol.* **2011**, *8*, 2279–2285. [CrossRef]
208. Hovsepian, P.E.; Kok, Y.N.; Ehiasarian, A.P.; Haasch, R.; Wen, J.G.; Petrov, I. Phase separation and formation of the self-organised layered nanostructure in C/Cr coatings in conditions of high ion irradiation. *Surf. Coat. Technol.* **2005**, *200*, 1572–1579. [CrossRef]
209. Yi, P.Y.; Peng, L.F.; Zhou, T.; Wu, H.; Lai, X.M. Development and characterization of multilayered Cr-C/a-C:Cr film on 316L stainless steel as bipolar plates for proton exchange membrane fuel cells. *J. Power Sources* **2013**, *230*, 25–31. [CrossRef]
210. Gamburzev, S.; Appleby, A.J. Recent progress in performance improvement of the proton exchange membrane fuel cell (PEMFC). *J. Power Sources* **2002**, *107*, 5–12. [CrossRef]
211. Maricle, D.; Nagle, D. Carbon Foam Fuel Cell Components. U.S. Patent 4,125,676, 14 November 1978.
212. Kumar, A.; Reddy, R.G. Materials and design development for bipolar/end plates in fuel cells. *J. Power Sources.* **2004**, *129*, 62–67. [CrossRef]

213. Tang, Y.; Yuan, W.; Pan, M.Q.; Wan, Z.P. Feasibility study of porous copper fiber sintered felt: A novel porous flow field in proton exchange membrane fuel cells. *Int. J. Hydrog. Energy* **2010**, *35*, 9661–9677. [CrossRef]
214. Tseng, C.J.; Tsai, B.T.; Liu, Z.S.; Cheng, T.C.; Chang, W.C.; Lo, S.K. A PEM fuel cell with metal foam as flow distributor. *Energy Convers. Manag.* **2012**, *62*, 14–21. [CrossRef]
215. Yuan, W.; Tang, Y.; Yang, X.; Wan, Z. Porous metal materials for polymer electrolyte membrane fuel cells—A review. *Appl. Energy* **2012**, *94*, 309–329. [CrossRef]
216. Verma, A.; Pitchumani, R. Analysis and optimization of transient response of polymer electrolyte fuel cells. *J. Fuel Cell. Sci. Technol.* **2015**, *12*, 1–10. [CrossRef]
217. Lin, R.; Xiong, F.; Tang, W.C.; Techer, L.; Zhang, J.M.; Ma, J.X. Investigation of dynamic driving cycle effect on the degradation of proton exchange membrane fuel cell by segmented cell technology. *J. Power Sources* **2014**, *260*, 150–158. [CrossRef]
218. Xu, L.F.; Li, J.Q.; Ou Yang, M.G.; Hua, J.F.; Yang, G. Multi-mode control strategy for fuel cell electric vehicles regarding fuel economy and durability. *Int. J. Hydrog. Energy* **2014**, *39*, 2374–2389. [CrossRef]
219. Kheirandish, A.; Kazemi, M.S.; Dahari, M. Dynamic performance assessment of the efficiency of fuel cell-powered bicycle: An experimental approach. *Int. J. Hydrog. Energy* **2014**, *39*, 13276–13284. [CrossRef]
220. Hou, Y.P.; Yang, Z.H.; Fang, X. An experimental study on the dynamic process of PEM fuel cell stack voltage. *Renew. Energy* **2011**, *36*, 325–329. [CrossRef]
221. Durst, J.; Lamibrac, A.; Charlot, F.; Dillet, J.; Castanheira, L.F.; Maranzana, G.; Dubau, L.; Maillard, F.; Chatenet, M.; Lottin, O. Degradation heterogeneities induced by repetitive start/stop events in proton exchange membrane fuel cell: Inlet vs. outlet and channel vs. land. *Appl. Catal. B Environ.* **2013**, *138*, 416–426. [CrossRef]
222. Reiser, C.A.; Bregoli, L.; Patterson, T.W.; Yi, J.S.; Yang, J.D.L.; Perry, M.L.; Jarvi, T.D. A reverse-current decay mechanism for fuel cells. *Electrochem. Solid State Lett.* **2005**, *8*, A273–A276. [CrossRef]
223. Shen, Q.; Hou, M.; Liang, D.; Zhou, Z.; Li, X.; Shao, Z.; Yi, B. Study on the processes of start-up and shutdown in proton exchange membrane fuel cells. *J. Power Sources* **2009**, *189*, 1114–1119. [CrossRef]
224. Brightman, E.; Hinds, G. In situ mapping of potential transients during start-up and shut-down of a polymer electrolyte membrane fuel cell. *J. Power Sources* **2014**, *267*, 160–170. [CrossRef]
225. Li, H.Y.; Weng, W.C.; Yan, W.M.; Wang, X.D. Transient characteristics of proton exchange membrane fuel cells with different flow field designs. *J. Power Sources* **2011**, *196*, 235–245. [CrossRef]
226. Yu, Y.; Li, H.; Wang, H.J.; Yuan, X.Z.; Wang, G.J.; Pan, M. A review on performance degradation of proton exchange membrane fuel cells during startup and shutdown processes: Causes, consequences, and mitigation strategies. *J. Power Sources* **2012**, *205*, 10–23. [CrossRef]
227. Hou, M.; Yu, H.M.; Yi, B.L. Current Status and Perspective of Vehicular Fuel Cell Technologies. *Prog. Chem.* **2009**, *21*, 2319–2332.
228. Manokaran, A.; Pushpavanam, S.; Sridhar, P. Dynamics of anode-cathode interaction in a polymer electrolyte fuel cell revealed by simultaneous current and potential distribution measurements under local reactant-starvation conditions. *J. Appl. Electrochem.* **2015**, *45*, 353–363. [CrossRef]
229. Liang, D.; Shen, Q.; Hou, M.; Shao, Z.G.; Yi, B.L. Study of the cell reversal process of large area proton exchange membrane fuel cells under fuel starvation. *J. Power Sources* **2009**, *194*, 847–853. [CrossRef]
230. Verma, A.; Pitchumani, R. Effects of operating parameters on the transient response of proton exchange membrane fuel cells subject to load changes. *Int. J. Hydrog. Energy* **2014**, *39*, 19024–19038. [CrossRef]
231. Park, S.; Jung, D. Effect of operating parameters on dynamic response of water-to-gas membrane humidifier for proton exchange membrane fuel cell vehicle. *Int. J. Hydrog. Energy* **2013**, *38*, 7114–7125. [CrossRef]
232. Zhang, Z.Q.; Jia, L.; Wang, X.; Ba, L.M. Effects of inlet humidification on PEM fuel cell dynamic behaviors. *Int. J. Energy Res.* **2011**, *35*, 376–388. [CrossRef]
233. Dubau, L.; Castanheira, L.; Maillard, F.; Chatenet, M.; Lottin, O.; Maranzana, G.; Dillet, J.; Lamibrac, A.; Perrin, J.C.; Moukheiber, E.; et al. A review of PEM fuel cell durability: Materials degradation, local heterogeneities of aging and possible mitigation strategies. *Wiley Interdiscip. Rev. Energy Environ.* **2014**, *3*, 540–560. [CrossRef]
234. Yan, X.Q.; Hou, M.; Sun, L.Y.; Cheng, H.B.; Hong, Y.L.; Liang, D.; Shen, Q.; Ming, P.W.; Yi, B.L. The study on transient characteristic of proton exchange membrane fuel cell stack during dynamic loading. *J. Power Sources* **2007**, *163*, 966–970. [CrossRef]

235. Yu, P.T.; Gu, W.; Makharia, R.; Wagner, F.T.; Gasteiger, H.A. The impact of carbon stability on PEM fuel cell startup and shutdown voltage degradation. *ECS Trans.* **2006**, *3*, 797–809.
236. Owejan, J.E.; Yu, P.T.; Makharia, R. Mitigation of carbon corrosion in microporous layers in PEM fuel cells. *ECS Trans.* **2007**, *11*, 1049–1057.
237. Huang, C.; Li, C.; Shi, G. Graphene based catalysts. *Energy Environ. Sci.* **2012**, *5*, 8848–8868. [CrossRef]
238. Ioroi, T.; Senoh, H.; Yamazaki, S.I.; Siroma, Z.; Fujiwara, N.; Yasuda, K. Stability of corrosion-resistant Magnéli-phase Ti_4O_7-supported PEMFC catalysts at high potentials. *J. Electrochem. Soc.* **2008**, *155*, B321–B326. [CrossRef]
239. Chhina, H.; Campbell, S.; Kesler, O. High surface area synthesis, electrochemical activity, and stability of tungsten carbide supported Pt during oxygen reduction in proton exchange membrane fuel cells. *J. Power Sources* **2008**, *179*, 50–59. [CrossRef]
240. Zhao, S.; Wangstrom, A.E.; Liu, Y.; Rigdon, W.A.; Mustain, W.E. Stability and Activity of Pt/ITO Electrocatalyst for Oxygen Reduction Reaction in Alkaline Media. *Electrochim. Acta* **2015**, *157*, 175–182. [CrossRef]
241. Balliet, R.J.; Reiser, C.A.; Patterson, T.W.; Perry, M.L. Start up System and Method for a Fuel Cell Power Plant Using a Cathode Electrode Fuel Purge. U.S. Patent 6,838,199, 4 January 2005.
242. Hideaki, K. Fuel cell system and fuel cell system control method. WO2,008,146,122, 23 May 2008.
243. Fellows, R. System and method for minimizing fuel cell degradation after shutdown. U.S. Patent 9,231,261, 5 January 2002.
244. Falta, S.R.; Lang, M.A.; Di Fiore, D.C. Anode purge and drain valve strategy for fuel cell system. U.S. Patent 9,105,888, 11 August 2015.
245. Van Dine, L.L.; Steinbugler, M.M.; Reiser, C.A.; Scheffler, G.W. Procedure for shutting down a fuel cell system having an anode exhaust recycle loop. U.S. Patent 6514635 B2, 4 February 2011.
246. Ramani, M.; Bodner, D.; Miller, M.; Schnitzer, M.; Miklas, R. Methods of treating fuel cells and fuel cell systems. U.S. Patent 20050136298 A1, 23 June 2005.
247. Wu, X.X.; Xu, H.F.; Lu, L.; Fu, J.; Zhao, H. The study on dynamic response performance of PEMFC with RuO2•xH2O/CNTs and Pt/C composite electrode. *Int. J. Hydrog. Energy* **2010**, *35*, 2127–2133. [CrossRef]
248. He, J.; Ahn, J.; Choe, S.Y. Analysis and control of a fuel delivery system considering a two-phase anode model of the polymer electrolyte membrane fuel cell stack. *J. Power Sources* **2011**, *196*, 4655–4670. [CrossRef]
249. Abdullah, M.; Idres, M. Fuel cell starvation control using model predictive technique with Laguerre and exponential weight functions. *J. Mech. Sci. Technol.* **2014**, *28*, 1995–2002. [CrossRef]
250. Patterson, T.W., Jr.; Darling, R.M. Avoiding fuel starvation of anode end fuel cell. WO2013126075 A1, 29 August 2013.
251. Harris, D.I.; Lang, M.A.; di Fiore, D.C. Anode Gas Composition Utilizing h2 Injection Pressure Wave Propagation Rates. U.S. Patent 2,012,028,152A1, 10 December 2014.
252. Yan, X.; Hou, M.; Sun, L.; Liang, D.; Shen, Q.; Xu, H.; Ming, P.; Yi, B. AC impedance characteristics of a 2 kW PEM fuel cell stack under different operating conditions and load changes. *Int. J. Hydrog. Energy* **2007**, *32*, 4358–4364. [CrossRef]